

**OPTICAL AND STRUCTURAL STUDIES OF ANODIC COPPER PIGMENTED  
TITANIUM PHOTOCATALYST**

**BY**

**PETER CORMACK OWINO**

**A THESIS SUBMITTED IN PARTIAL FULFILLMENT OF THE  
REQUIREMENTS FOR THE AWARD OF DEGREE OF MASTER OF SCIENCE  
IN THE SCHOOL OF SCIENCE, UNIVERSITY OF ELDORET, KENYA**

**DECEMBER, 2020**

## DECLARATION

### Declaration by the candidate

This thesis is my own original work and has not been submitted for any academic award in any institution; and shall not be reproduced in part or full, or in any format without prior written permission from the author and/or University of Eldoret.

**Peter Cormack Owino**      **Signature:** ..... **Date:** .....  
**SC/PGP/007/15**

### Declaration by Supervisors

This thesis has been submitted with our approval as University supervisors.

**1. Prof. Mghendi Mwamburi** **Signature:** ..... **Date:** .....

**University of Eldoret, Kenya**

**2. Dr. David Waswa**      **Signature:** ..... **Date:** .....

**University of Eldoret, Kenya**

**DEDICATION**

To my father George Mc. Juma for his love and care throughout my life, my wife Lucy Atieno for standing with me through the rough and tough times, my son and daughter Brandon Juma and Precious Angel Akinyi whom I owe for their love and support.

## ABSTRACT

Thousands of lives have been lost worldwide due to the shortage of clean water resources caused by waste water disposal challenges from manufacturing and processing industries, population growth and long-term droughts. In Kenya, the disposal of organic pollutants and colored water from industries has become a major challenge both to the humans and the environment. This has led to the study of titanium dioxide (TiO<sub>2</sub>) photocatalysis as an advanced oxidation process with a potential for practical application in water treatment over other treatment technologies. In this study, commercial pure grade 1 titanium foils measuring 6 cm × 3 cm were used to fabricate anodic TiO<sub>2</sub> films at different time intervals by anodization at 200 V in a mixture of 0.5 M sulphuric acid, hydrofluoric acid and distilled water at inter-plate distances of 1 cm. An electrodeposition cell was prepared using a 0.1 M CuSO<sub>4</sub>.5H<sub>2</sub>O electrolyte solution, and thereafter pigmentation of the anodized plate was done at 12 V for a period of 5 s and annealed in muffle furnace for a period of 4 hours at a temperature of 450 °C. The determination of both the surface and optical characteristics of the anodic TiO<sub>2</sub> films were done using Lambda 9 UV/VIS/NIR Spectrophotometer, Fourier Transform Infrared Spectroscopy, Atomic Force Microscopy, X-ray diffraction (XRD) and Scanning Electron Microscopy. The XRD measurements confirmed the presence of both rutile and anatase phases in TiO<sub>2</sub> films. The photocatalytic performances of the films were assessed by the photo-degradation of 10 ppm methylene-blue solution under UV irradiation. Methylene-blue was used in place of the industrial waste water effluent containing dye because of its ability to lend easily to spectroscopic analysis. The optimum anodization time for the films with a high photocatalytic activity in the degradation of methylene blue for this study was found to be 2 minutes.

**TABLE OF CONTENTS**

DECLARATION .....	ii
ABSTRACT .....	iv
TABLE OF CONTENT .....	v
LIST OF TABLES .....	viii
LIST OF FIGURES .....	ix
LIST OF SYMBOLS .....	xii
LIST OF ABBREVIATIONS AND ACRONYMS .....	xiv
ACKNOWLEDGEMENT .....	xv
CHAPTER ONE .....	1
INTRODUCTION .....	1
1.1 Overview .....	1
1.2 Introduction .....	1
1.3 Water pollution.....	2
1.4 Titanium oxide (TiO <sub>2</sub> ) Films.....	3
1.5 Statement of the problem .....	3
1.6 Objectives of the study.....	4
1.7 Rationale.....	5
1.8 Hypotheses .....	5
1.9 Significance of the study .....	5
CHAPTER TWO .....	7
LITERATURE REVIEW .....	7
2.1 Introduction .....	7
2.2 Discovery of Photocatalysis.....	7
2.3 Photocatalytic Reaction.....	8
2.4 Oxidation Process.....	9
2.5 Reduction Process .....	10
2.6 Parameters Affecting Photocatalysis.....	11

2.6.1	Crystal Structure and Surface topology of the Catalyst.....	12
2.6.2	Temperature .....	12
2.6.3	Acidity.....	13
2.6.4	Light Intensity.....	13
2.6.5	Amount of Catalyst.....	14
2.6.6	Concentration of Pollutants in Wastewater.....	14
2.7	Photocatalyst .....	15
2.8	Determination of the photocatalytic rate .....	17
2.9	Photocatalytic Decolorization Using Ultra Violet (UV) Radiation .....	19
2.10	Anodization .....	22
2.11	Formation of colour by thin films .....	26
2.12	Pigmentation.....	29
2.13	Annealing .....	32
2.14	Optical Properties of Dielectric Films.....	34
2.15	Transmittance and Reflectance .....	36
2.16	Dyes.....	38
2.17	Concerns of textile dyeing effluents.....	43
CHAPTER THREE .....		43
METHODOLOGY .....		44
3.1	Introduction .....	44
3.2	Experimental methods.....	44
3.2.1	Pretreatment of titanium substrate .....	44
3.2.2	Anodic oxidation of Titanium (IV) Oxide films.....	44
3.2.3	Pigmentation of Titanium plate .....	46
3.2.4	Annealing of Titanium plates.....	47
3.2.5	Spectral reflectance measurement.....	48
3.2.6	Fourier-transform infrared spectroscopy (FTIR) .....	49
3.2.7	Atomic Force Microscopy (AFM) .....	51
3.2.8	Scanning Electron Microscopy (SEM) .....	52
3.2.9	X – Ray diffractometer (XRD) .....	53
3.2.10	Photocatalysis. ....	53

CHAPTER FOUR.....	59
RESULTS AND DISCUSSION .....	59
4.1    Introduction .....	59
4.2    Effect of anodizing time on color formation of the oxide films.....	59
4.3    Effect of anodization time on current.....	61
4.4    Optical properties of anodic TiO <sub>2</sub> films .....	62
4.4.1    Reflectance measurement of anodic TiO <sub>2</sub> films.....	62
4.4.2    Fourier-transform infrared (FTIR) spectroscopy measurement.....	65
4.4.3    X-ray diffraction measurement .....	68
4.5    Surface characteristics of TiO <sub>2</sub> films .....	71
4.5.1    Atomic Force Microscopy (AFM) .....	71
4.5.2    Surface roughness .....	74
4.5.3    Scanning Electron Microscopy (SEM) .....	78
4.6    Photo-catalytic measurement .....	80
CHAPTER FIVE .....	83
CONCLUSION AND RECOMMENDATION.....	83
5.1    Introduction .....	83
5.2    Conclusion.....	83
5.3    Recommendation for further work.....	84
REFERENCE.....	85
APPENDIX I : SIMILARITY REPORT .....	96

**LIST OF TABLES**

<b>Table 1.</b>	Characteristics of typical raw textile dyeing mill effluents.....	40
<b>Table 2.</b>	Classes of dyes according to color index (C.I.).....	42
<b>Table 3.</b>	Anodization time in comparison to refractive index and thickness.....	65
<b>Table 4</b>	Effect of anodization time on the average crystallite size (D), dislocation density ( $\delta$ ) and micro strain ( $\epsilon$ ) of the samples.....	71



## LIST OF FIGURES

<b>Figure 2.1</b>	Redox process of a photocatalytic reaction.....	9
<b>Figure 2.2</b>	Oxidation process of a photocatalytic reaction.....	10
<b>Figure 2.3</b>	Pairing reaction of oxygen during the reduction process.....	11
<b>Figure 2.4</b>	Colours achievable through anodization of titanium.....	26
<b>Figure 2.5</b>	Formation of thin film interference.....	27
<b>Figure 2.6</b>	Light beam impinging at interface between different media.....	37
<b>Figure 2.7</b>	Reflectance and transmittance waves at media interface.....	37
<b>Figure 3.1</b>	Experimental set up for anodization of TiO <sub>2</sub> plate.....	45
<b>Figure 3.2</b>	Electrodepositing set up for pigmentation.....	47
<b>Figure 3.3</b>	Shows the annealing furnace with (A) samples ready for heat treatment and (B) furnace set at 450 °C for 4 hours with samples inside.....	47
<b>Figure 3.4</b>	Schematic diagram of reflectance measurement using integrating Sphere.....	48
<b>Figure 3.5</b>	Perkin Elmer (UV/VIS/NIR Lambda 9) Photo-spectrometer set up.....	49
<b>Figure 3.6</b>	Fourier transform infra-red spectroscopy (Platinum FTR).....	50
<b>Figure 3.7</b>	Shows (A) computer processing raw data and (B) FTIR spectrometer with an attenuated total reflectance ATR attachment.....	50
<b>Figure 3.8</b>	Atomic force microscopy set – up in operation.....	51
<b>Figure 3.9</b>	Atomic force microscope and (B) Image of the sample's morphology displayed by the monitor.....	52
<b>Figure 3.10</b>	Photocatalytic reactor equipment.....	54
<b>Figure 3.11</b>	Photocatalytic reactor base.....	55

<b>Figure 3.12</b>	(A) Photoreaction unit and (B) top view of photoreaction unit cuvette.....	55
<b>Figure 3.13</b>	Inside of photoreaction unit cuvette.....	56
<b>Figure 3.14</b>	(A) UV source and (B) UV source cooling fan.....	56
<b>Figure 3.15</b>	Lutron UV-340 UV light meter.....	57
<b>Figure 3.16</b>	(A) Reactor in the sun and (B) Photocatalytic data acquisition unit.....	58
<b>Figure 4.1</b>	Samples anodized between 20 s and 120 s.....	59
<b>Figure 4.2</b>	Samples anodized from 1 min to 30 min.....	60
<b>Figure 4.3</b>	Effect of time on the current pattern.....	62
<b>Figure 4.4</b>	Reflection spectra of TiO <sub>2</sub> thin film a function of wavelength.....	63
<b>Figure 4.5</b>	FTIR measurement of pure titanium.....	66
<b>Figure 4.6</b>	FTIR spectra of TiO <sub>2</sub> anodized at different time intervals.....	67
<b>Figure 4.7</b>	XRD patterns of TiO <sub>2</sub> films anodized for different time intervals.....	69
<b>Figure 4.8</b>	Effect of anodization time on the morphology of the samples, (A) un-anodized Ti (B) 1 min (C) 2 min (D) 3 min (E) 10 min and (F) 30 min.....	72
<b>Figure 4.9</b>	Surface morphology of sample taken at different positions and anodized for 30 min.....	74
<b>Figure 4.10</b>	Comparison of samples surface roughness against anodizing time (A) the average surface roughness (Ra) and (B) root mean square of the sample roughness (Rms).....	75
<b>Figure 4.11</b>	Surface cross-section of (A) un-anodized Ti sample (B) anodized at 1 min.....	76
<b>Figure 4.11</b>	(C) anodized at 2 min (D) anodized at 3 min (E) anodized at 10 min.....	77
<b>Figure 4.11</b>	(F) anodized at 30 min.....	77

<b>Figure 4.12</b>	SEM images for the samples anodized for (A) 1 min (B) 2 min (C) 3 min (D) 10 min and (E) 30 min.....	79
<b>Figure 4.13</b>	Absorbance spectra for TiO <sub>2</sub> films anodized at different time intervals.....	81

**LIST OF SYMBOLS**

$a$	Absorptivity
$D$	Average crystallite size
$e^-$	Electron (charge carrier)
$E_I$	Incident energy
$E_R$	Reflected energy
$f$	Frequency
$H_2$	Hydrogen
$H^+$	Hydrogen ion
$h^+$	Hole (charge carrier)
$I$	Incident radiation
$I_A$	Absorbed radiation
$I_R$	Reflected radiation
$I_T$	Transmitted radiation
$k_{i,j}$	Complex extinction coefficient
$t$	Thickness
$T$	Transmittance
$V$	Applied Voltage
$\Delta$	Path difference
$\beta$	Full width at half maximum (FWHM)
$\delta$	Dislocation density
$\varepsilon$	Micro strain
$n_a$	Refractive index of air
$n_f$	Refractive index of TiO <sub>2</sub> film
$n_s$	Refractive index of titanium substrate

$n_{i,j}$	Refractive index
$n_{p,i,j}$	Refractive index for P polarized light wave
$\lambda_0$	Wavelength in vacuum
$\lambda_j$	Wavelength of light in the oxide film
$\lambda_n$	Wavelength of light in a medium of refractive index $n$
$\theta$	Braggs angle
$\theta_{i,j}$	Angle of incidence in radians
$\omega$	Angular frequency

**LIST OF ABBREVIATIONS AND ACRONYMS**

A	Absorbance
AC	Alternating current
AFM	Atomic Force Microscopy
ASD	Anodic Spark Deposition
ATR	Attenuated Total Reflection
BGY	Brilliant Golden Yellow
CB	Conduction band
C.I	Colour index
DC	Direct current
eV	Electron volt
FT-IR	Fourier Transform Infrared
M	Molar
MB	Methylene blue
MAO	Micro-Arc Oxidation
SEM	Scanning electron microscopy
STI	Science, technology and innovation
UV	Ultraviolet
UV/VIS/IR	Ultraviolet-Visible-Infra red
VB	Valence band
VLA	Visible light active
XRD	X-ray diffraction

## ACKNOWLEDGEMENT

First of all, my sincere gratitude is to the Almighty God for His sustenance and life throughout my studies.

I wish to sincerely thank my supervisors Prof. Mghendi Mwamburi and Dr. David Waswa for their guidance and invaluable suggestions that went a long way to make this work a success. The constant availability and supervision, wise counsel and corrections were necessary for objectivity. I am indebted to the University of Eldoret for the opportunity to advance my studies in the institution especially the Physics department, Chemistry department and the Soil Science department for their cooperation in the provision of equipment and other necessities that were important to carry out the experiments.

I wish also to sincerely thank the following;

The International Science Programs (ISP), Upssala University, Sweden for the facilitation towards this research work.

Material Science and Solar Energy for Eastern and Central Africa (MSSEESA), University of Dar es Salaam where some of this work was carried out; I wish also to extend my gratitude to the following persons, Dr. M. E. Samiji, Dr N. R. Mlyuka, Dr. G. A. Kinunda and Eng Khalfan for their guidance and support.

# CHAPTER ONE

## INTRODUCTION

### 1.1 Overview

This chapter gives a brief review on water treatment using other conventional biological methods and their shortcomings which led to the study of titanium dioxide (TiO<sub>2</sub>) as a photocatalyst, its significance and justification of the study.

### 1.2 Introduction

Effluent streams from textile and other manufacturing industries using dyeing processes are considered to have a higher percentage of colour in them (Kumar *et al*, 2016). These dyes are normally poisonous to the humans, plants and aquatic life when discharged to the water bodies (Chong *et al*, 2010). Studies have shown that the traditional methods of water purification are ineffective for decolorizing such effluent streams from industries due to the stability of the dyes used in the process of manufacturing finished products (Chong *et al*, 2010). This prompted researchers to study other possible methods of decolorizing effluent streams from industries which include adsorption, chemical coagulation, chlorination and ozonation (Punyasloka *et al*, 2018). Adsorption and chemical coagulation merely removes the physical component of dye from the waste water effluent without degrading it completely, thereby causing a problem in waste disposal. Chlorination and ozonation degrades dye from the coloured waste water effluent by synthetic response. Both chlorine and ozone are solid, non-particular oxidizers that debase the organic compounds of dye when introduced to the waste water streams. However, the disposal of the organic compounds from chlorinated waste water to the environment is highly discouraged and regulated. Ozonation is a more efficient



water cleaning method though very costly due to the high electrical power needed to necessitate the generation of O<sub>3</sub> onsite which is chemically unstable. Ozone, is considered more hazardous when in contact with the environment, therefore, a destructive unit needs to be in place to forestall the unreacted O<sub>3</sub> from getting away into the environment (Kalaivani and Suja, 2016).

### **1.3 Water pollution**

Colour is one of the major perceptible markers of water tainting. The disposal of highly coloured waste water effluent to the water bodies results into a great damage to aquatic life (Chatzisyneon *et al*, 2013). The centralization of dye might be lower compared to any other chemical disposed in the effluent stream but its strong color makes it more visible thus causing serious aesthetic and pollution problems. Worldwide, roughly 15% of the engineered material colors are directed to streams during the way toward assembling (Silva and Faria, 2003).

Therefore, much attention and research has been placed on methods that decolour and degrade dyes from textile effluents completely. Among the existing methods, heterogeneous photocatalysis with TiO<sub>2</sub> semiconductor has received much attention as a high level oxidation measure due to as a high level oxidation measure due to its ability to operate at ambient conditions, lack of mass transfer limitations and use of solar radiation (Batt *et al*, 2018). So far, studies have been done on the photocatalytic corruption of model colors, for example, Remazol Black B within the sight of ultraviolet (UV) solar radiation (Chatzisyneon *et al*, 2013). However, few reports exit on the photocatalytic corruption of genuine (recreated) color effluents utilizing TiO<sub>2</sub> under sunlight based radiation (Chatzisyneon *et al*, 2013).

#### **1.4 Titanium oxide (TiO<sub>2</sub>) Films**

Titanium dioxide (TiO<sub>2</sub>) films have been generally contemplated in view of their interesting photocatalytic properties compared to other semiconductor devices. Over the years, TiO<sub>2</sub> thin films have shown a remarkable range of applications in various fields like defensive coatings, antibacterial and optical coatings, and gas detecting and dielectric films for another age field impact transistor among others. (Chan *et al*, 2011).

TiO<sub>2</sub> is a photosensitive semiconductor which induces an inter-band transition when photon energy equal to or higher than the band-hole energy of the semiconductor is absorbed by its crystal structure. During the process of inter-band transition, the photogenerated pairs achieve charge separation and gain enough energy to move to the surface of the TiO<sub>2</sub> film. These charge carriers respond with air and water to deliver OH extremists and O anions, which in the long run assault the natural mixes adsorbed on the outside of TiO<sub>2</sub> plates and eliminate them by changing into CO<sub>2</sub> and H<sub>2</sub>O. Thus, the surface of TiO<sub>2</sub> films act as a strong oxidizer which attacks the organic compounds adsorbed on it, cleaning both water and air through a process known as photodestruction (Li and Zhang, 1996).

#### **1.5 Statement of the problem**

The demand for clean water resources worldwide has become a major issue due to the rapid growth of manufacturing and processing industries with poor disposal mechanisms of waste water effluent, population growth and long-term droughts. In Kenya, the lack of proper disposal mechanisms of organic pollutants in waste water effluents from manufacturing and processing industries and the inadequacy in efficient water cleaning methods has been a major challenge both to humans and the environment. One of the

major pollutants that finds itself into the water bodies from industries such as textiles, cosmetics, food, plastic, pharmaceutical, paper, food and tanneries among other industries are dyes which are a significant class of manufactured natural mixes (Kumar *et al*, 2016). The waste water gushing from the industries to the water bodies containing dye cause a major challenge in the development of aquatic life; this happens when the sunlight incident to the polluted water is adsorbed and reflected by the colour content in dye. Research shows that the focal sensory system in people and animals can be affected by these organic pollutants as well as cause skin disturbance, blood issue, liver and kidney harm (Chong *et al*, 2010). Currently, mechanisms such as chemical coagulation, adsorption and ozonation do not completely degrade dye but convert them into another phase without being totally destroyed (Kalaivani and Suja, 2016). On the other hand, customary water treatment strategies, for example, sedimentation and filtration alongside compound and film innovations include high working expenses and could produce poisonous auxiliary toxins into the ecosystem (Chong *et al*, 2010). In this project, studies are done to determine the impact of anodization time on the photocatalytic action of copper pigmented anodic TiO<sub>2</sub> photocatalyst.

### **1.6 Objectives of the study**

The main objective of this research is to study the effect of anodization time on the preparation of copper pigmented anodic TiO<sub>2</sub> photo catalyst and test its efficiency using a standard methylene blue solution. The specific objectives are:-

1. To fabricate TiO<sub>2</sub> films by anodization.
2. To determine the optimum anodization time for TiO<sub>2</sub> films.
3. To determine the surface and optical properties of the samples.

4. To determine the photocatalytic performance of anodic  $\text{TiO}_2$  through photodegradation of methylene blue using a photocatalytic reactor in the presence of natural UV radiation.

### **1.7 Rationale**

This project will help in meeting Kenya's goal of affordable and efficient cleaning water technique. The key economic deliverables namely; Universal healthcare, Manufacturing, Affordable housing and Food security all round up to the availability of clean water both for industrial, agricultural and domestic use. The economic and social policies needed to achieve these goals are dependent upon the adoption of Science, technology and Innovation (STI) as an implementation tool to clean water and sanitation which on the other hand will reduce the many deaths witnessed every year connected to water borne diseases.

### **1.8 Hypotheses**

The chemical and structural stability of titanium dioxide ( $\text{TiO}_2$ ) as well as its phase composition makes it the most favorable semiconductor for photocatalysis compared to other semiconducting oxides.

Anodic titanium dioxide ( $\text{TiO}_2$ ) films degrades harmful natural mixes, diminish metal-particles, improve the biodegradability in cellulose effluents and decolour an incredible assortment of colors in arrangement or in strong blends.

### **1.9 Significance of the study**

In this study, the best preparation parameters are established for the creation of anodic  $\text{TiO}_2$  films. The proficiency of this films and their application in the degradation of

colour in waste water will help in solving the challenges caused due to environmental degradation as a result of poor disposal mechanisms from processing and manufacturing industries. Secondly, it will contribute to enhanced technology and innovation on how to improve on the properties of  $\text{TiO}_2$  as a suitable photocatalyst.

## CHAPTER TWO

### LITERATURE REVIEW

#### 2.1 Introduction

This chapter investigates applicable writing audits and sets up the hypothetical reason for the investigation of titanium dioxide (TiO<sub>2</sub>) as the primary semiconductor photocatalyst. Summary of the redox process, parameters affecting photocatalysis, anodizing and annealing procedure is also discussed.

#### 2.2 Discovery of Photocatalysis

Fundamental examines have been done over the most recent 30 years with respect to the complexities of semiconductor photocatalysis. In 1972, a discovery on the phenomenon of water purification using photocatalytic water parting on a TiO<sub>2</sub> film within the sight of ultraviolet (UV) light was done (Fujishima *et al*, 1972). This break through resulted in a series of studies in search of a better and more efficient photocatalytic method to produce H<sub>2</sub> fuel (Duong *et al*, 1984). This resulted to what was known as the hydrogen economy, leading to a 1973 oil crisis that in part, led to the modern water splitting method known as heterogeneous photocatalysis with TiO<sub>2</sub> as the main catalyst.

1980s presented an outstanding development of heterogeneous photocatalysis using TiO<sub>2</sub> semiconductor as a catalyst with emphasis on nanoparticles which saw several publications in 2010 focusing on the applications of TiO<sub>2</sub> photocatalysis in the environmental arena such as photodegradation of a large number of pollutants.

TiO<sub>2</sub> photocatalysis has been greatly debated between the periods of 1980 – 2000 regarding;

- a) The photocatalytic reaction mechanism (Oxidation versus Reduction process),
- b) Surface modification of the semiconductor (Increasing semiconductors' reaction sites),
- c) Parameters for efficient photocatalytic activity.

Since then, extensive research has been done in understanding the important mechanisms of increasing the photocatalytic efficiency of TiO<sub>2</sub> films. A majority of these studies considered water purification technique using TiO<sub>2</sub> photocatalyst as an attractive method for the complete decimation of natural mixes in waste water effluent (Chatzisyneon *et al*, 2013).

### **2.3 Photocatalytic Reaction**

The photon energy and the semiconductor catalyst are the main sensitizers for the illumination of light in a photocatalytic reaction that activates a redox process because of electrons move from the valence band to the conduction band (Hagen, 2006). This process is well illustrated in Figure 2.1.

The important facts to be noted about photocatalysis are (Chatzisyneon *et al*, 2013)

- a) The photon energy higher or then again equivalent to the band hole energy of the semiconductor invigorates electrons from the valence band to the conduction band.
- b) Holes in the valence band oxidize adsorbed substrates on the catalyst surface by reacting with the water molecules to produce hydroxyl revolutionaries which help in the debasement of contaminations in the water effluents.

- c) The electrons in the conduction band react with the separated oxygen to form superoxide particles which instigate the redox responses.

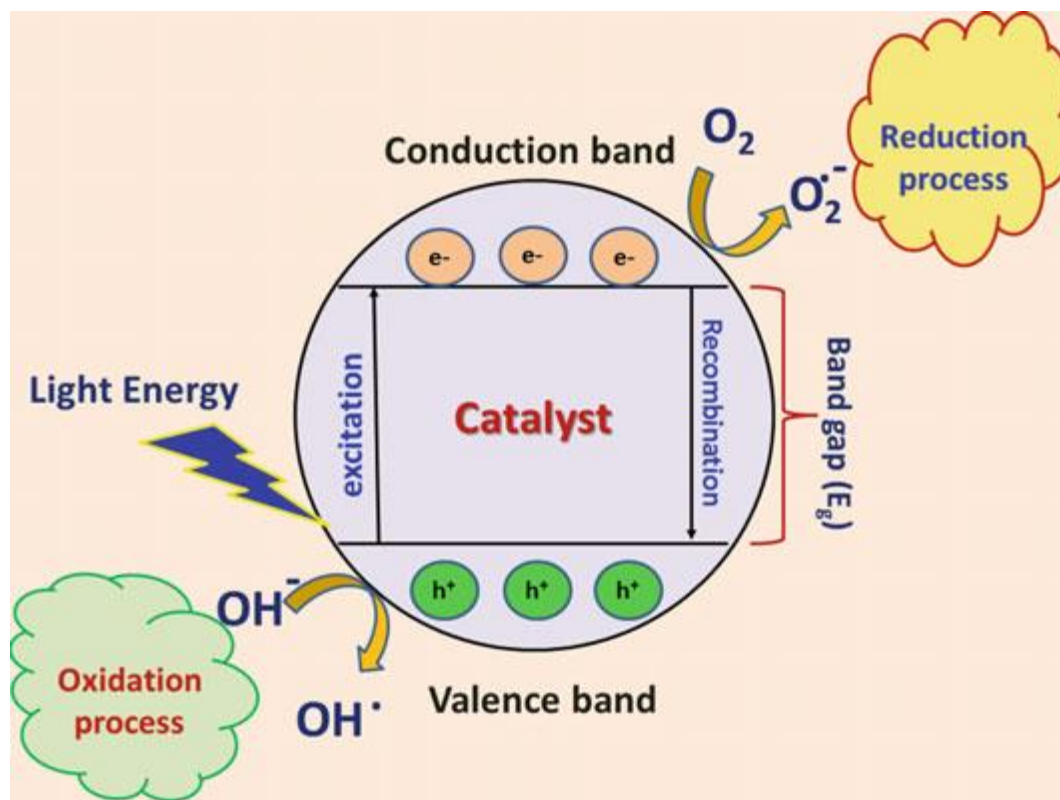


Figure 2.1: Redox process of a photocatalytic reaction (Khan *et al*, 2015)

## 2.4 Oxidation Process

In this process, openings in the valence band oxidize adsorbed water on the catalyst surface, eventually generating hydroxyl ( $\cdot\text{OH}$ ) radicals. The presence of oxygen in terms of superoxide ( $\text{O}^{\cdot-}$ ) anions is very important in the entire process. The generated hydroxyl ( $\cdot\text{OH}$ ) radicals and superoxide ( $\text{O}^{\cdot-}$ ) anions assault the natural mixes adsorbed on the photocatalyst surface breaking down them totally by changing into carbon dioxide and



water (Khan *et al*, 2015; Rajeshwar *et al*, 2008). Fig. 2.2 shows the process of oxidation on adsorbed organic compounds on the outside of the semiconductor.

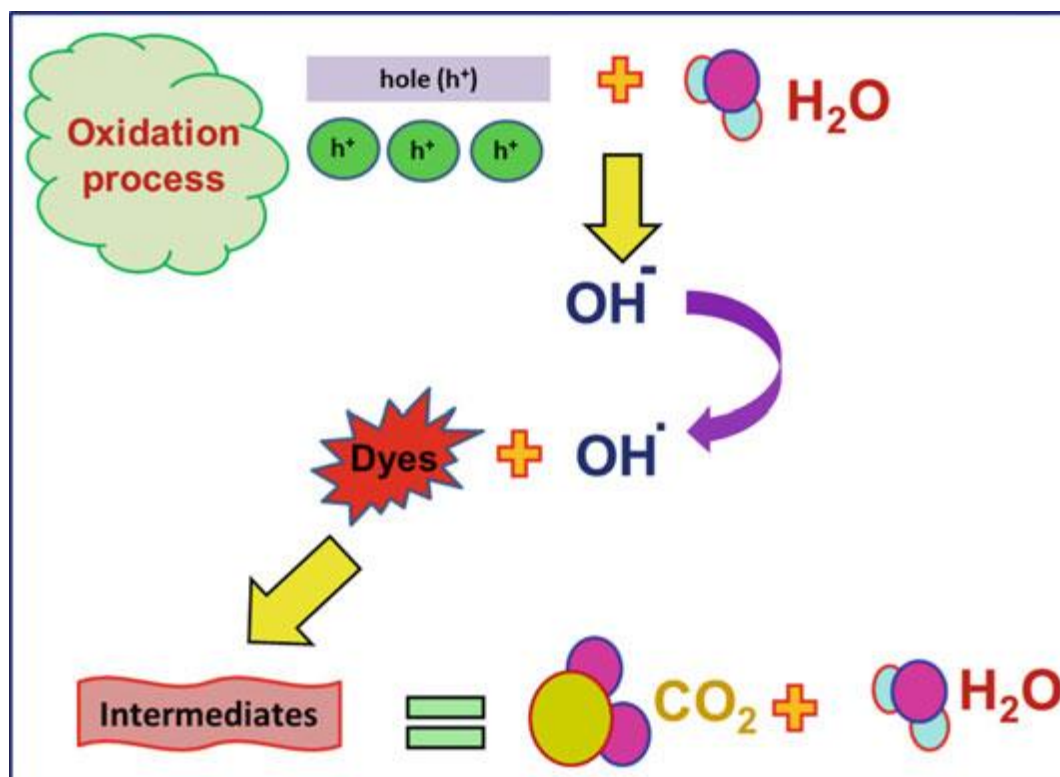
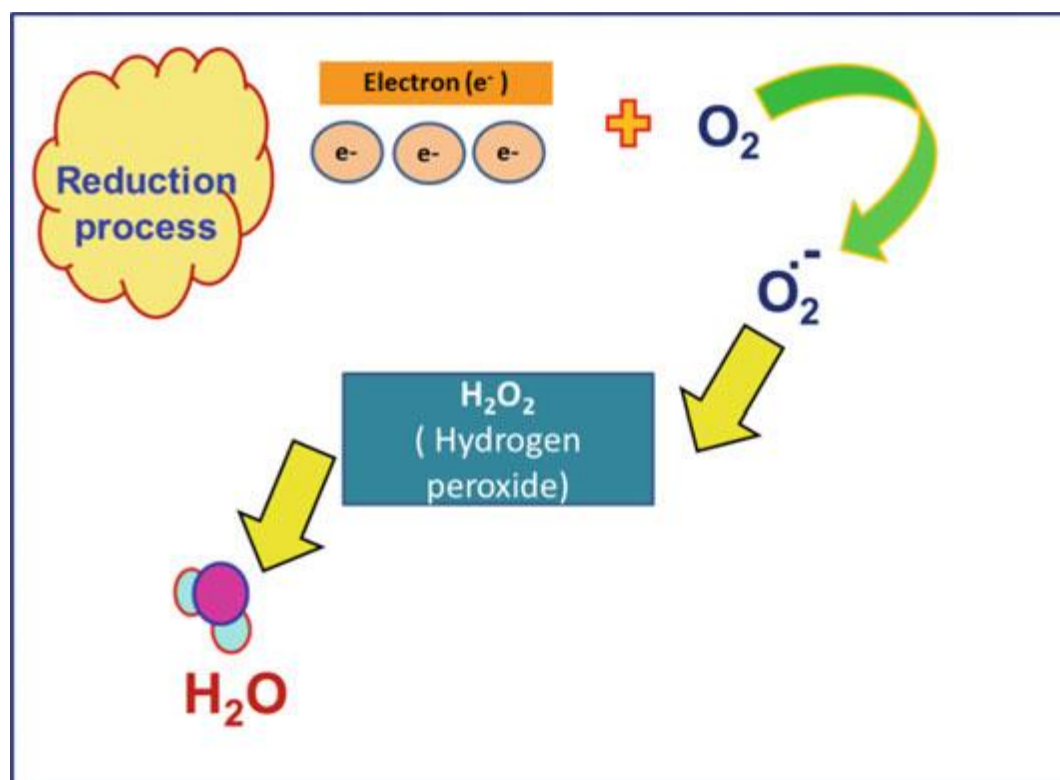


Figure 2.2: Oxidation process of a photocatalytic reaction (Khan *et al*, 2015)

## 2.5 Reduction Process

Figure 2.3 shows the pairing reaction of oxygen occurring during the process of reduction (Rajeshwar *et al*, 2008; Rehman *et al*, 2009). The conduction band electron reacts with the broke up oxygen to deliver a superoxide anion ( $O^\cdot$ ). The produced anion attached to the organic compound responds with the hydrogen particle to create hydrogen peroxide lastly transforms into water. The age of openings in the valence band are straightforwardly identified with the grouping of natural issue in the water. The higher

the centralization of the natural issue in the water, the higher the excitation of electrons from the valence band to the conduction band within the sight of UV light thus diminishes the recombination rate. This in turn creates more reaction sites in the semiconductor causing an efficient photocatalytic activity (Nakata and Fujishima, 2012; Khan *et al*, 2015).



**Figure 2.3: Pairing reaction of oxygen during the reduction process (Rehman *et al*, 2009)**

## 2.6 Parameters Affecting Photocatalysis

The following parameters assume a significant part in the pace of photodegradation of natural accumulates by photocatalytic water sanitization: gem structure and surface geography of the impetus, temperature, causticity, light power, measure of impetus, and

grouping of wastewater (Chatzisyneon *et al*, 2013). The details of how each of these parameters contribute to the photocatalytic process are given in sections 2.5.1 – 2.5.6

### **2.6.1 Crystal Structure and Surface topology of the Catalyst**

The precise structure of a semiconductor photocatalyst is one of the determinants for a superior photocatalytic action. TiO<sub>2</sub> materials solidifies in three stages in particular; rutile, anatase, and brookite. From research, the anatase stage has been discovered to be the most touchy and appealing stage with the best photocatalytic movement because of its dependability, adsorption power, the situation of the conduction band, and the more significant level of hydroxylation (Gnanasekaran *et al*, 2015). The surface and underlying morphology of the material additionally assumes a significant part in affecting the last corruption proficiency of the impetus (Wang *et al*, 2008). The nanosized TiO<sub>2</sub> materials having huge surface region and more modest size have been demonstrated to be more proficient for water cleaning and reusing capacity contrasted with the mass materials because of their more modest size (Han *et al*, 2014). At the point when the size of a semiconductor photocatalyst is more modest, an enormous number of molecules amass on its surface prompting an expansion in surface to volume proportion. This expands various response destinations and interfacial charge transporter move rates, subsequently accomplishing higher photocatalytic exercises (Cernuto *et al*, 2011).

### **2.6.2 Temperature**

Temperature greatly affects the photocatalytic output of the semiconductor during its preparation. The optimum range of reaction temperature for photocatalytic systems predominantly relies upon the energy infused into the material during the response. In this entire process, generation of heat is not necessary. TiO<sub>2</sub> photocatalytic activity

operates better at a temperature of between 20 – 80 °C (Chatterjee and Dasgupta, 2005). An expansion in the initiation energy of the material happens when the temperature is at 0 °C and underneath. At the point at the point when the temperature is raised more than 80 °C, the electron–opening recombination and desorption pattern of adsorbed reactant species additionally increments, coming about in to an abatement of photocatalytic movement (Chatterjee and Dasgupta, 2005).

### **2.6.3 Acidity**

The pH of a solution in photocatalytic reactions is an important factor in determining the surface charge properties of a photocatalyst and the efficiency of degradation of organic pollutants (Kazeminezhad and Sadollahkhani, 2016). The photocatalytic degradation rate of TiO<sub>2</sub> materials differ under different pH conditions. In the alkaline range (pH 11–13), an unexpected drop of degradation was reported because of the hydroxyl radicals (OH) that quickly rummaged and doesn't respond with dyes (Saravanan *et al*, 2017). The effect of pH can be deciphered regarding electrostatic communications between charged particles and the pollutants which impact the adsorption and in this way the surface properties.

### **2.6.4 Light Intensity**

The power of light assumes a significant job in deciding the pace of debasement of photocatalytic reactions. The measure of light consumed by the precious stone structure of the photocatalyst is given by the proportion of the photocatalytic response rate to the pace of assimilation of the photon energy (Saravanan *et al*, 2017). The pace of photocatalytic response shifts under various frequencies of the light source (Chatterjee and Dasgupta, 2005; Akpan and Hameed, 2009). The anatase phase of TiO<sub>2</sub>

semiconductor has a band gap of 3.2 eV which corresponds to the UV absorption region wavelength of 388 nm (Reza *et al*, 2015). The pace of debasement of the natural builds within the sight of light and TiO<sub>2</sub> as an impetus fluctuates for various powers of light. As the force of light expansion in the scope of 0 – 20 mW/cm<sup>2</sup>, the rate of reaction also increases. At high-intensity of light irradiation above 25 mW/cm<sup>2</sup>, the reaction rate decreases because of the expansion of recombination pace of electron–opening sets. (Saravanan *et al*, 2017).

### **2.6.5 Amount of Catalyst**

The proficiency of photocatalytic debasement is likewise impacted by the measure of impetus. If the quantity of catalyst is increased, the reaction sites also increases. This accelerates the generation of more hydroxyl radicals (OH) and superoxide anions (O<sup>-</sup>) resulting in an increase of the photocatalytic degradation rate (Saravanan *et al*, 2017). Studies have already demonstrated that the pace of corruption of the natural builds in the response is straightforwardly corresponding to the convergence of the impetus in any reactor framework (Konstantinou and Triantafyllos, 2004). Be that as it may, as the measure of impetus is expanded past an ideal focus, the debasement rate diminishes because of the decrease of the profundity infiltrated by light into the arrangement, thereby resulting to the occurrence of diminished light scattering.

### **2.6.6 Concentration of Pollutants in Wastewater**

The sort of toxin and its fixation assumes a vital part in the debasement pace of the natural compounds (Rajeshwar *et al*, 2008; Rehman *et al*, 2009; Malato *et al*, 2009). Numerous specialists doing photocatalytic action utilizing comparable impetuses under comparable working conditions yet with varieties in the fundamental grouping of water

impurities announced various outcomes because of the distinction in light time important to achieve total debasement of the natural mixes (Saravanan *et al*, 2017). It has been reported that the efficiency of TiO<sub>2</sub> semiconductor operating under same photocatalytic conditions but using different concentrations of acid differed. Further, studies have also established that, at higher concentration of dye, the degradation rate exponentially diminishes (Kiriakidou *et al*, 1999).

## **2.7 Photocatalyst**

Titanium and its photocatalytic properties were discovered in 1967 and later published in 1972 after an extensive research in this area (Fujishima *et al*, 1972). Titanium dioxide as a thin film semiconductor has a significant job in the creation of energy: as an impetus, TiO<sub>2</sub> parts water atoms into oxygen and hydrogen, with the gathered hydrogen being utilized as a fuel. Pigmenting TiO<sub>2</sub> with carbon greatly improves the efficiency of the photocatalytic process. Further creating imperfections to the grid structure of the surface layer of titanium dioxide nanocrystals enhances efficiency and durability, permitting absorption of infrared radiation (Chatterjee and Dasgupta, 2005).

In 1995, there was a discovery of the excess attraction of titanium dioxide (TiO<sub>2</sub>) films to water, a phenomenon known as superhydrophilicity. In this phenomenon, water in contact with the titanium dioxide film does not form any contact angle under light irradiation. Superhydrophilic materials such as TiO<sub>2</sub> have several advantages among which are the ability to defog glass, enable water to swipe away dust in form of oil easily hence leading to the manufacture of car mirrors, self-cleaning glass and against hazing coatings which lessen the centralization of airborne toxins, for example, unstable natural mixes and nitrogen oxide (Chatterjee and Dasgupta, 2005).

Research has shown that titanium dioxide exhibits a high photocatalytic activity compared to other semiconductor photocatalysts especially in its anatase phase under ultraviolet (UV) irradiation. This photoactivity appears more enhanced at the {001} planes of the crystal structure of anatase, even so, {101} planes have been found to be thermodynamically more steady and more noticeable in most orchestrated and normal anatase gem structure as obvious by the frequently noticed tetragonal dipyramidal development propensity. TiO<sub>2</sub> semiconductor with interfaces among rutile and anatase stage improve photocatalytic movement by encouraging charge transporter partition. Titanium dioxide having two periods of anatase and rutile have upgraded usefulness as a photocatalyst. Studies have indicated that doping titanium dioxide with either nitrogen particles or metal oxide like tungsten trioxide, improves photoexcitation within the sight of noticeable light (Neppolian et al, 2002). The openings made in the valence band after the excitation of electrons have solid oxidative potential that oxidizes water into hydroxyl extremists. The openings can likewise oxidize oxygen or natural materials straightforwardly. Subsequently, notwithstanding its utilization as a hydrolysis impetus, titanium dioxide can likewise be utilized in different applications, for example, color, be added to paints, tiles, or different items for its cleaning, freshening up and against fouling properties (Hussein and Asadi, 2016).

TiO<sub>2</sub> has a great advantage in industrial applications on water and air purification due to the following factors (Konstantinou and Triantafyllos, 2004):

1. Its ability to degrade waste water effluent in the presence of solar radiation and oxygen under ambient conditions.

2. The unique properties of TiO<sub>2</sub> photocatalyst including its chemical and mechanical stability.
3. Its efficiency in the total destruction of organic compounds making it safe both to the humans and the environment.
4. Degrade organic compounds changing them to H<sub>2</sub>O and CO<sub>2</sub>.

The total photodestruction of organic matter from air and water is also experienced in antimicrobial coatings. These are thin film coatings applied to surfaces and furniture which have the ability to photodegrade fungi, virus and bacteria attached to them (Konstantinou and Triantafyllos, 2004).

## **2.8 Determination of the photocatalytic rate**

Methylene blue (MB) is normally used because it lends easily to spectroscopic analysis (Skooq *et al*, 2011). The concentration of MB is determined by passing light through the cuvette. The absorption of the light energy from the incident beam passing through the analyte is corresponding to the grouping of the slution.

Reflection occurs at the two wall-solution interfaces in a transparent cuvette or cell, with the resulting beam attenuation being substantial. In addition, weakening of a shaft may happen because of dispersing by enormous atoms in the arrangement and now and again from retention by the dividers of the container (Li *et al*, 2005). To make up for these impacts, the intensity of the shaft sent by the analyte solution is generally contrasted and the intensity of the bar communicated by an indistinguishable cell containing the dissolvable as it were. An exploratory set up is in this manner significant in the



determination of conditions that intently surmised the genuine conveyance (T) and absorbance (A) in a reaction process, i.e,

$$T = \frac{P_{\text{solution}}}{P_{\text{solvent}}} \approx \frac{P}{P_0} \quad 2.1$$

$$A = \log \frac{P_{\text{solvent}}}{P_{\text{solution}}} \approx \log \frac{P_0}{P} \quad 2.2$$

Transmission of light through the analyte is reduced when its particles or atoms take up the energy of a photon of light bringing about the event of light retention (Gaya and Abdullah, 2008). As light goes through clear materials and additionally arrangements, it weakens dramatically. This decrease of sent light is straightforwardly extent to the grouping of the arrangement just as the way length of light voyaged. Thus,

$$\%T = [(Transmitted\ Light) / (Incident\ Light)] * 100$$

According to the law of Conservation of energy, the total incident radiation (I) can be equated as the sum of the reflected ( $I_R$ ), transmitted ( $I_T$ ), and absorbed ( $I_A$ ) radiations. Thus,

$$I = I_R + I_T + I_A$$

The lessening of the communicated beam in agreement to Beer-Lambert's law can be characterized in a homogeneous, non-diffusing and retaining medium as:

$$\log \left( \frac{I_T}{I} \right) = abc \quad 2.3$$

Absorbance (A) is directly related to transmittance (T) which is a ratio of  $\left(\frac{I}{I_0}\right)$ . This means that,

$$A = \log\left(\frac{I_0}{I}\right) \quad 2.4$$

Beer-Lambert Law relates absorbance to the negative logarithmic capacity, base 10, of the conveyance saw by an example, which brings about a straight relationship to the force of the engrossing species and the distance went by light.

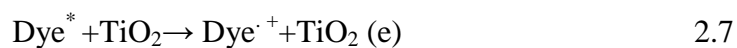
$$\text{Absorbance} = -\text{Log}_{10}(T) \quad 2.5$$

Beer's law relates the absorption pattern of the solution in regards to the analyte concentrations. It is important to note that, high analyte focuses ( $>0.01$  M), the degree of solute-dissolvable connections, solute-solute cooperation's, or hydrogen holding can influence the arrangement's current circumstance and its absorptivity (Skooq *et al*, 2011).

## 2.9 Photocatalytic Decolorization Using Ultra Violet (UV) Radiation

Photocatalytic responses by semiconductors are subject to the photograph acceptance of electron-opening sets by band opening radiation that completes in redox reactions at the outside of the photocatalyst. The most standard semiconductor is TiO<sub>2</sub> with a band opening width of 3.2 eV (identifying with absorbance at 388 nm). The photon energy is consumed by the precious stone structure of TiO<sub>2</sub> material bringing about the excitation of an electron from the valence to conduction band subsequently forsaking an opening. The openings at the valence band have a positive redox capability of + 2.6 V which responds and oxidize adsorbed water particles to deliver hydroxyl revolutionaries. Then again, oxygen responds with the electron in the conduction band to create a superoxide

anion extremist (O<sub>2</sub><sup>-</sup>). The common responses that happen through photograph excitation (by means of assimilation of light at  $\lambda > 440$  nm) of color particles and excitation of electrons into the conduction band of titanium to deliver oxidizing species, for instance, superoxide, peroxy and hydroxyl progressive are yielded in conditions 2.6 – 2.11 (Foo and Hameed, 2010).



A variety of colors have been accounted for to be oxidized by TiO<sub>2</sub>/UV treatment. Saggiaro et al, (2011), exhibited the photocatalytic corruption of headstrong colors, for example, Reactive Red 239 and Reactive Black 5 utilizing 0.1 g L<sup>-1</sup> of powdered TiO<sub>2</sub>. He saw that the pace of photodegradation was higher under acidic pH. The outcomes were clarified based on expanded electrostatic fascination between SO<sub>3</sub>-gatherings of Reactive Black 5 color and positive charges on the TiO<sub>2</sub> surface. Out of the different metal oxides, ZnO can retain light similar to 425 nm and is viewed as the most appropriate other option. Powerful decolorization and corruption of Brilliant Golden Yellow (BGY) color was accounted for by Habib et al, (2013) utilizing ZnO - TiO<sub>2</sub>

nanocomposite powder at different molar proportions. A significant issue with TiO<sub>2</sub> powder is the regular recombination of electron/opening sets which lessens the general productivity of photocatalytic degradative responses. A powerful methodology to battle this issue is the expansion of other elective electron acceptors, for example, H<sub>2</sub>O<sub>2</sub> at low fixations. Another genuine restriction is the accumulation of fine titanium powder and its misfortune into the treated water. This issue was overcome by the improvement of immobilized impetus utilizing support networks, for example, earth, sand, silica gel and actuated carbon. Foo and Hameeed, (2010), introduced a condition of craftsmanship audit on the utilization of TiO<sub>2</sub>/enacted carbon composites and its application for the corruption of colors, to be specific Methyl Blue, Methyl Orange, Reactive Red X-38, Acridine Orange, Indigo Carmine and Rhodamine. The degree of expulsion of different introductory groupings of colors went from 81% to 100%. Li et al, (2005) and Zhang et al, (2005) upheld on the photocatalytic execution of TiO<sub>2</sub>/initiated carbon concerning debasement of methyl orange which was kept up even after 10 response cycles.

Muruganandham *et al*, (2006), compared the advanced oxidative decolorization of Reactive Yellow 14 azo dye by UV/H<sub>2</sub>O<sub>2</sub>, UV/TiO<sub>2</sub> and UV/H<sub>2</sub>O<sub>2</sub>/Fe<sup>2+</sup> processes and reported on the decolourization efficiencies of these cycles in the accompanying request UV/H<sub>2</sub>O<sub>2</sub>/Fe<sup>2+</sup> > UV/TiO<sub>2</sub> > Fe<sup>2+</sup>/H<sub>2</sub>O<sub>2</sub> > UV/H<sub>2</sub>O<sub>2</sub>. The advantages of photooxidative degradation responses are:

- a) No slop creation and
- b) Decrease of awful stench.

The impediments of photocatalytic oxidation are:

- c) High operational expense and
- d) Failure of UV light to penetrate reliably into effluents containing chromophoric mixes accordingly lessening the viability of the cycle.

### **2.10 Anodization**

This is an electrolytic passivation measure used to grow the thickness of the ordinary oxide layer outwardly of the catalyst. The use of anodization in the year 1923 opened a new error in the industrial revolution. In those early years, this process was used mostly to safeguard Duralumin sea plane parts from corrosion and was recorded in the British defense specification coded as DEF STAN 03-24/3. The year 1927, ushered a new patent on the use of sulfuric acid as the main electrolyte in anodization. Sulfuric acid has since been the most commonly used electrolyte since then (Edwards, 1997).

In Germany, the process of anodization was used greatly in the construction industry with anodized aluminium extrusion as the main architectural material. In 1960's and early 1970's opened an avenue for research in this area leading to the displacement of anodized aluminium with cheaper plastics and powder coatings in the construction industries. Apart from sulfuric acid, phosphoric acid has likewise been extraordinarily utilized as an electrolyte in the pre-treatment for adhesives or organic paints. Since its discovery, anodization has been greatly used in the industry not only to prevent metals from corrosion but also to enhance their application in different fields'e.g. for water purification (Sul *et al*, 2001).

The electrolyte anodization takes place in a set-up of an electrochemical cell having two electrode systems with the cathode being a metal that does not react with the electrolyte.

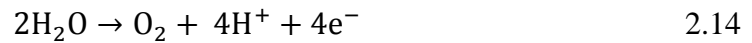
The application of a consistent voltage or current between the anode and cathode causes a chain of reactions (redox reaction) which prompts the making of an oxide film of changing thickness on the outside of the anodic semiconductor dependent upon factors like anodization voltage, time, concentration of electrolyte and temperature due to field-driven ion diffusion.

Anodization of titanium undergoes the following chemical reactions (Sul *et al*, 2001).

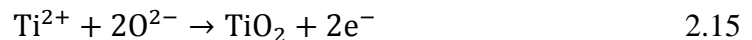
At the Ti/TiO<sub>2</sub> interfaces:



Reactions at the interfaces of Ti oxide/electrolyte are:



At both interfaces:



The circuit current drops during the formation of the oxide film on the surface of the anodic Ti plate because of the high opposition brought about by the developing oxide layer in comparison to the electrolyte and the metal substrate. The oxide layer on the Ti metal plate continues to grow as long as the applied electrical field is sufficient to move the ion conduction through the oxide (Sul *et al*, 2001). A relation of the growth of the oxide layer thickness,  $t$ , to the applied voltage ( $V$ ) can be established as,

$$t \approx aV \quad 2.16$$

Where  $a$  is a constant in the range of 1.5-3 nm/V

The development of a nanoporous layer on the titanium oxide film is controlled by the three cycles in particular, field-upgraded oxidation, field–helped oxidation and compound oxide disintegration. During field–improved oxidation, the oxide layer is kept on to the titanium metal, as oxygen particles move towards the interface of the metal and its oxide in the solution. Field-assisted oxide dissolution operates in the reverse; in this process, the titanium ions from the metal-oxide interface migrate through the oxide layer and disintegrate into the solution. The presence of Hydrofluoric acid (HF) in the solution is to accelerate the rate of oxide dissolution by consuming titanium ions in solution and the creation of pores on the Ti sample (Gong *et al*, 2001). This process enhances pore widening, while the extensive dissolution of the oxide layer over long anodization periods prompts pore blending and the possible loss of the nanopores structure.

The process of anodization can be carried out either at constant current or constant voltage. If the voltage applied between the anode and cathode terminals of the set up surpasses the restriction of dielectric breakdown of the oxide, the oxide layer won't have the option to oppose flow moving through it, accordingly prompting a nonstop improvement of a comparative oxide layer onto the metal surface of the semiconductor. This process results into more sparking and gas evolution, a process known as Anodic Spark Deposition (ASD) or Micro-Arc Oxidation (MAO). From research,  $H_2SO_4$  and  $H_3PO_4$  have been found to have breakdown potentials of 100 V and 80 V respectively, and most cases, the thickness of the oxide layer is to a great extent controlled by these

breakdown limits. Taking  $\text{H}_2\text{SO}_4$  into consideration, the anodic oxide film is usually thick and porous above its breakdown limits of 100 V, and this trend applies for all non-fluorine electrolytes. Under relatively low voltages, Fluoride ions tend to generate nanopores on the surface of the Ti semiconductor (Malekshahi *et al*, 2013). Temperature then again, assumes a significant job in the development of a homogeneous oxide layer on the metal surface during the cycle of anodization. A steady temperature keeps a homogeneous field-upgraded disintegration measure over the whole region of the semiconductor surface while chemical dissolution rate on the same oxide layer is accelerated by increased temperature. To forestall an absolute disintegration of the oxide layer, the working temperature should be kept relatively low.

The mechanism of Anodic Spark Deposition (ASD) can be explained using the avalanche theory (Malekshahi *et al*, 2013). The oxide film formed in the process of anodization goes about as a dielectric boundary that forestalls the progression of current through it. The growth of the oxide layer continues until reaching the dielectric breakdown limit after which it begins to dissolve to the bottom of the electrolyte. The oxide film thickness on the anodized plate isn't uniform because of the presence of imperfections, deformities and nearby stresses on the atoms of the semiconductor film. Sparking during the anodization process takes place due to the potential drop experienced at the frail points of the electrode when the dielectric limit is exceeded as a result of increased applied voltage. The temperature at these weak points rapidly increases, leading to a local melting process. The increase of temperature at these weak points generates heat, thus causing thermal stress to the anodic material resulting to the multiplication of frail points (Gong *et al*, 2001).



Fundamentally, the development of the oxide layer on the anodic surface is controlled by the distinction in the pace of arrangement of the oxide film to the pace of disintegration of a similar film given by the idea of electrolyte. Anodization boundaries, for example, applied voltage, current thickness, pH and electrolyte concentration are directly connected to the nature of the electrolyte (Sul *et al*, 2001).

### 2.11 Formation of colour by thin films

Anodized titanium creates a variety of shadings relying upon various components among which are; the anodizing voltage, Time, Electrolyte focus and temperature. The shading shaped relies upon the thickness of the oxide layer kept on the semiconductor. These tones are framed because of the impedance of light at the air – oxide interface and the oxide – metal interface.



**Figure 2.4: Colours achievable through anodization of titanium (Edwards, 1997).**

The thickness of the oxide layer can be estimated in the range of a few micrometers. Anodized titanium has found applications in dental implants, costume jewelry, metal coatings, jewelry and wedding rings as well as in photocatalysis (Edwards, 1997). Standards for titanium anodizing are given by AMS 2487 and AMS 2488.

When titanium metal is anodized at different voltages, different colours are formed on the metal plates due to the interference of the light reflected at the air-oxide interface and the light reflected at the metal substrate-oxide interface (Edwards, 1997). These colours represent a thin oxide film of varying thickness dependent on the anodizing voltage

formed on the metal plates. There are many other similar phenomena in nature, for example, the colours produced by thin soap films on water and the colours of thin film oil spills on water.

Accepting that light strikes the oxide film of thickness  $t$  and refractive index  $n_f$  at close to normal incidence, the accompanying set up realities are considered:

1. A light wave going from a medium of lower refractive index to a medium of higher refractive index consequently goes through a phase change of  $\pi$  ( $180^\circ$ ) upon reflection. A light wave going from a medium of higher refractive index to one of lower refractive index experiences no phase change upon reflection.

2. The wavelength of light  $\lambda$  in a medium of refractive index  $n$  is given by  $\lambda_n = \frac{\lambda_0}{n}$ , where  $\lambda_0$  is the wavelength in vacuum or, approximately, in air.

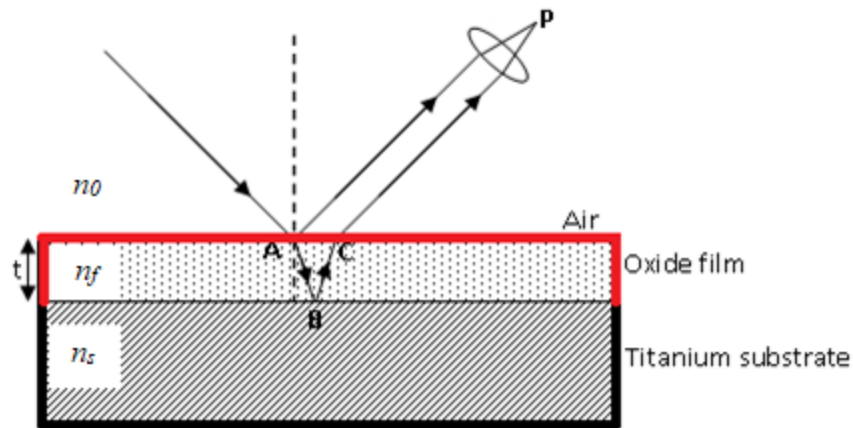


**Figure 2.5: Formation of thin film interference (Sul *et al*, 2001)**

Figure 2.5, shows an incident light beam of index  $n_0$  from the air going through a straightforward film of index  $n_f$ . The oxide film on the metal substrate of index  $n_s$  splits the

incident light at A into reflected portion to point P and refracted portion to point B. The light beam refracted at point A is further reflected at the metal - oxide interface (point B) to point C which is the air - oxide interface and further reflected to point P. Part of the beam from point B to C experiences multiple reflections within the oxide layer until its intensity diminish.

Due to the complex nature of multiple reflections taking place within the oxide layer, the two emerging parallel light beams exiting the oxide layer from points A and C which are converged at point P are considered.

The two beams from point A and C intersecting at P overlap and interfere. A relative phase difference is developed by the two beams voyaging various ways from point A and C, one in air, the other somewhat in the film along these lines creating useful or ruinous obstruction at P.

In the event that the incident beam is almost opposite to the surface, the way distinction (AB + BC) is around equivalent to double the film thickness  $2t$ .

Then,

$$\Delta = n(AB + BC) = n(2t) \quad 2.17$$

Where  $t$  is the film thickness,  $\Delta$  is the optical path difference and  $n$  is the index of the medium. If  $2nt = \lambda_0$ , the wavelength of the light in air, the two interfering beams as a result of their optical path difference alone would be in phase and produce helpful obstruction.

Thus, the equation for constructive interference becomes;

$$\text{Normal incidence: } 2n_f t + \frac{\lambda_o}{n} = m\lambda_o, (m = 1, 2, 3 \dots) \quad 2.18$$

If  $n_f > n_o$  and  $n_f > n_s$ , the reflection at B, occurs for light going from a higher index  $n_f$  toward a lower index  $n_s$ . Hence, the light reflected at A shifts phase by  $180^\circ$  while the light reflecting at B does not. If  $2nt = \lambda_o$  is added, a total optical path difference of  $(\lambda_o + \frac{\lambda_o}{n})$  is attained due to the additional  $\frac{\lambda_o}{n}$  phase shift for the beam reflecting at A, leading to destructive interference. Thus,

The equation for destructive interference becomes;

$$\text{Normal incidence: } 2n_f t + \frac{\lambda_o}{n} = (m + \frac{1}{2})\lambda_o, (m = 1, 2, 3, \dots) \quad 2.19$$

If the colour is known, then the thickness can be estimated by these relationships.

## 2.12 Pigmentation

This is a process where materials or dyes are deposited in the pores of the anodic semiconductor plates or by dispersing particles in the anodic plates to achieve colour. Among the methods used to colour anodic oxide films, the electrolytic method is considered quite efficient and reliable. In this method, an alternating electric current is applied at low voltage and the metal ions are deposited at the bottom of the pores of the anodic film. The electrolyte consists of a mixture of the salt of the target metal mixed with de-ionized water. The thickness and pore structure of the anodized film regulates the colouring rate and distribution.

During the process of electrolytic colouring, an alternating current is passed through the anodic semiconductor with the copper plate as a counter electrode. These currents cause the copper in the presence of copper II sulphate electrolyte to be deposited into the pores of the anodic semiconductor, beginning from the base of the semiconductor and building upwards (Kang *et al*, 1999). The pores created during longer anodization period together with the barrier layer of the anodic semiconductor create a current path during pigmentation, which greatly affects current efficiencies that cause metal deposition during pigmentation. These greatly affect the efficiencies of the current causing metal deposition, which determines the uniformity and colour intensity of the final product.

Several methods have been used in enhancing the efficiency of photocatalytic titanium dioxide films ( $\text{TiO}_2$ ). These can be categorized as either;

- a) Surface alteration, deals with modifications of surface area against reaction sites of the material
- b) Chemical treatment, by adding other metals that alter the crystal and optical properties of the material.

Chemical modification of  $\text{TiO}_2$  photocatalysts has a greater advantage in controlling the morphology of the semiconductor and enhancing its overall efficiencies in the process of photocatalysis (Kang *et al*, 1999).

Pigmenting  $\text{TiO}_2$  films with progress metals like Cr, Co, V and Fe builds its phantom band all the way into the noticeable locale of the sun powered radiation prompting an improved photocatalytic movement (Czoska *et al*, 2008). Change metals have been found to cause warm flimsiness in  $\text{TiO}_2$  films because of their conduct in making

recombination locales for the photograph instigated charge transporters along these lines, bringing down its quantum proficiency. Despite a major achievement in reducing the band gap energy of semiconductors through metal doping, Kang *et al*, (1999) explains that photocatalysis is not enhanced due to lack of proper incorporation of the metal ions into the TiO<sub>2</sub> framework hence blocking the reaction sites on the surface of the semiconductor. Kang *et al*, (1999) further compares the effect of doping TiO<sub>2</sub> with Cr to TiO<sub>2</sub> with both Cr and V ion. Cr was discovered to reduce the photocatalytic activity while TiO<sub>2</sub> doped with both Cr and V ion implanted in it showed an increased photocatalytic activity compared to undoped TiO<sub>2</sub> for the disintegration of NO under sun oriented illumination (Morikawa et al, 2006). Another procedure includes adjusting TiO<sub>2</sub> with change metals, for example, Fe, Mn, Mo, Ru Cu, Co, Ni, Cr, V, Nb, W, Pt and Au. The presentation of progress metals in the precious stone structure of the anodic titanium dioxide film results on occasion to the making of new energy levels between valence band (VB) and conduction band (CB), inciting a move of light ingestion towards the noticeable light district. The sum, nature and sort of the doping specialist decide the rate and proficiency of Photocatalytic movement. Honorable metals like Ag, Au, Pt and Pd saved on the outside of TiO<sub>2</sub> films go about as electron traps subsequently improving the proficiency of photocatalytic action under noticeable light of the sunlight based radiation, which thus advances interfacial charge move and in this manner postponing recombination of the electron–opening sets (Wang et al, 2008). Platinum kept on TiO<sub>2</sub> traps photograph produced electrons, and accordingly increment the photograph actuated electron move rate at the interface. Then again, TiO<sub>2</sub> films pigmented suing Ag were found to improve photocatalysis in the obvious light range while the decrease of Ag on

TiO<sub>2</sub> during openness to noticeable light outcomes in excitation and converse electron stream from silver to the TiO<sub>2</sub> films subsequently oxidizing silver ( $\text{Ag} \rightarrow \text{Ag}^+$ ) simultaneously. The obvious light responsiveness of TiO<sub>2</sub> was certify to the surface plasmon reverberation of silver nanoparticles (Nolan et al, 2010).

Maeda and Yamada, (2007), announced that TiO<sub>2</sub> films doped with Cu demonstrated a higher photocatalytic action contrasted with different metals within the sight of noticeable light, while Fe-and Al-doped movies scarcely indicated any photocatalytic action. The optical ingestion spectra for the non-doped and metal-doped TiO<sub>2</sub> films show that compelling band hole narrowing is seen in the Fe-and Cu-doped TiO<sub>2</sub> films. It was additionally noticed that there is a higher recombination pace of the photogenerated electron/opening sets in the Fe-doped TiO<sub>2</sub> films, while successful charge partition of photogenerated electron/opening sets happens in the Cu-doped TiO<sub>2</sub> film. Al doping into the TiO<sub>2</sub> film has scarcely any impact on the photocatalysis of TiO<sub>2</sub> films (Maeda and Yamada, 2007).

### **2.13 Annealing**

Annealing is a heat treatment process for a specific duration and temperature being applied to a material that adjusts the physical and now and again synthetic properties of the material to build its pliability, relax it, assuage interior anxieties and insecurities to get better optical properties, such as in TiO<sub>2</sub> films (Ye *et al*, 2007). During the process of annealing, atoms migrate in the lattice structure of the material. As the heated material cools, the atoms re-arrange themselves in a least energetic manner, resulting in crystals with few dislocations leading to the decrease of both the dislocation density and the lattice imperfection. The rate of cooling determines the size of the crystals formed.

Higher cooling rate results in small crystals while a low cooling rate gives the atoms enough time to pack well. Required properties of the material can only be achieved when they are heated above their recrystallization temperature then given enough time to cool under an inert condition. Recrystallization is the cycle by which twisted grains are supplanted by another arrangement of undeformed ones that nucleate and develop until the first grains have been completely burned-through. Recuperation is the cycle by which distorted grains can lessen their put away energy by the expulsion or improvement of imperfections in their gem structure. The reduction in dislocations leads to improved electrical conductivity. At high temperature, there is deformation as the atoms vibrate and as the solid cools dislocations are reduced by new low energy arrangement of atoms (Fujishima *et al*, 2000).

For many materials, the phase composition and crystal grain size are dependent on the heating temperature and cooling rate. From research, the best annealing temperature has been established to be above 400 °C depending on the type of crystal structure needed. This reduces the dislocation density, implying a decrease in lattice imperfection due to the increase in crystallite size (Edwards, 1997).

Hou *et al*, (2003) reports that annealed anatase TiO<sub>2</sub> films have refractive index in the range of 2.10 - 2.50. The process of annealing causes the refractive index to increase due to the enhancement of crystallization.

The impact of strengthening treatment on the photocatalytic movement of TiO<sub>2</sub> created through different cycles was researched (Ohno *et al*, 2003). Molecule size or precious stone size was found to increment alongside structure change during the treatment



(Beltran et al, 2006). The grouping of sulphuric corrosive in the anodizing electrolyte assumes a significant part in the assurance of the crystallite size of the anatase period of the precious stone structure of TiO<sub>2</sub> film independent of strengthening. The as-anodized oxide shows a bigger crystallite size than that of the tempered oxide. Then again, the centralization of sulphuric corrosive doesn't influence the crystallite size of rutile period of TiO<sub>2</sub> semiconductor which is roughly 30 nm, and no express contrast is found between the as-anodized and toughened oxide (Nakane *et al*, 2003).

## **2.14 Optical Properties of Dielectric Films**

In semiconductors and dielectrics, the main absorption process occurs during the interaction of photon energy with electrons. This process takes place right when the semiconductor is enlightened with photon energy fit for energizing an electron from the valence band to the conduction band surface; for this situation the photon energy is then consumed by the precious stone structure of the semiconductor. The material is viewed as straightforward to photon radiation unequipped for energizing an electron to a higher state. Non-metallic solids have a little energy band hole contrasted with the semiconductors (Oganov and Lyakhov, 2010). The band to band advances of electrons establish the most grounded wellspring of ingestion. The valence electrons of dielectric materials, for example, glass, quartz, a few salts, jewel, many metal oxides, and most plastic materials are so firmly bound making it outlandish for an excitation to happen in the noticeable range. Then again, photons with energy in the bright can free them. In metals, huge densities of free electrons move openly restricting the presence of an electric field inside the strong. This property makes it a decent reflector and locate various optical applications among which are in the production of mirrors (Oganov and Lyakhov, 2010).

Semiconductors have properties that lie between those of metals and separators. These optical properties makes them straightforward in the close to infrared locale of the sun oriented radiation and furthermore engrossing in the obvious range with ingestion edge roughly between 0.5 eV ( $\lambda \sim 2500$  nm) and 2.5 eV ( $\lambda \sim 500$  nm), while dielectrics have solid retention in the bright district (Liu et al, 2013). The straightforwardness of semiconductor and dielectric materials is generally influenced by debasements, free electrons or openings in the conduction band and other deformity states at light illumination lower than the band-hole energy.

The saved optical movies can be ordered into two structures with unmistakable highlights. Microcrystalline structures made by the arrangement of haphazardly situated precious stones with the size equal to the request for the thickness of the oxide layer and the indistinct material whose translucent structure shapes a blemished occasional cluster organization of molecules. In microcrystalline materials, the locales between crystallites (grain limits) are exceptionally blemished with huge thickness of free electron energy states at energy levels which are between the valence and conduction groups. These imperfection states on the outside of the material empower light catching and retention subsequently energizing free electrons from the valence to the conduction band. The assimilation because of these imperfections is anyway more modest contrasted with that of the principal edge, yet it might influence the optical properties of the film (Allam et al, 2008).

In dielectric materials, periodicity of the precious stone structure assumes a significant job in deciding its optical properties. The presence of free electron states is dictated by the precious stone issue inside the band-hole. These free electron states are of two sorts: coordination deserts, additionally called hanging bonds or profound imperfections, just as valence and conduction band tail states (shallow states). These two electron states add to the ingestion of light energy. The shapeless dielectrics and semiconductors have a lot bigger ingestion coefficient because of band to band changes contrasted with their translucent guardians prompting more advances between electron states with an energy detachment equivalent to the photon energy. The testimony strategies just as the affidavit conditions are a primary determinant to the thickness of imperfection states and furthermore the relating optical assimilation strength.

### **2.15 Transmittance and Reflectance**

Figure 2.6 shows a sketch of a monochromatic beam of light impinging onto dielectric slim layers upheld by a thick substrate. The beam is partly transmitted, partly reflected and some of the radiation may be internally absorbed depending on the photon energy and layer thickness. This happens when there is a discontinuity in medium of transmission, mainly a change in optical density. At times, a change of phase occurs during reflection (Akira *et al*, 2008).

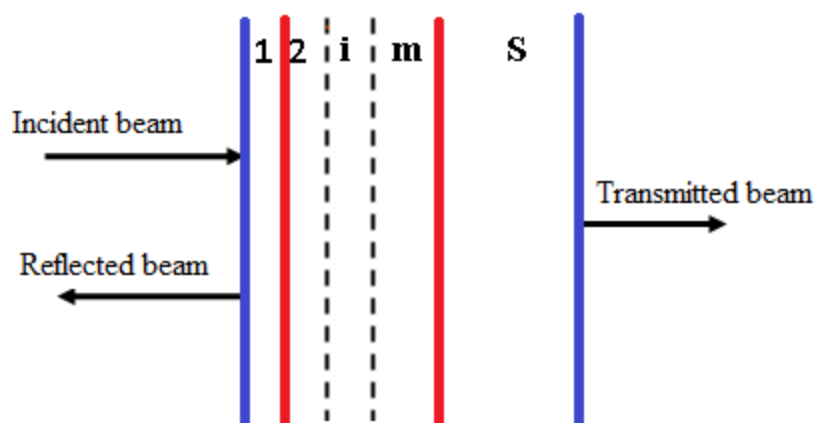


Figure 2.6: Light beams impinging at interface between different media (Sul *et al*, 2001)

For many layers, there is partial reflectance and transmittance hence, the aggregate sum of light reflected and transmitted by the structure results from the arithmetical amount of the amplitudes of these mostly reflected and partially transmitted beams.

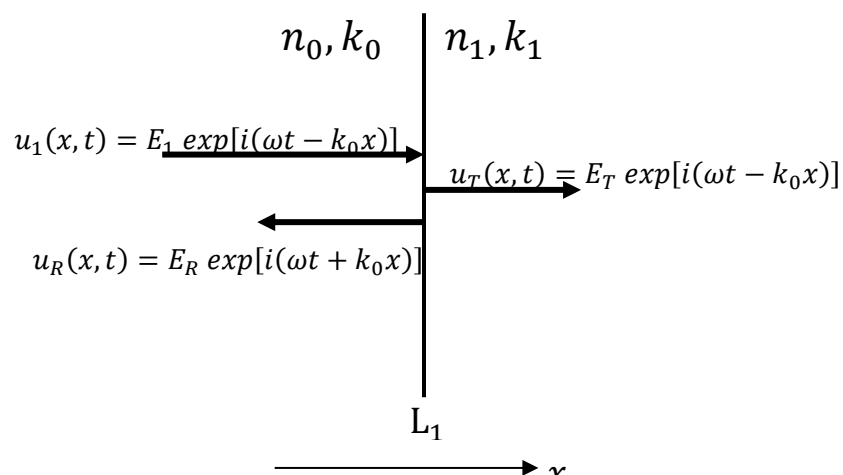


Figure 2.7 Reflected and transmitted waves at media interface

The wave functions from Figure 2.7 can be used to calculate the equations of both the transmittance and reflectance which are mainly used to decide the pace of colour degradation in the process of photocatalysis.

The function of the incident wave is;

$$u_1(x, t) = E_1 \exp[i(\omega t - k_0 x)] \quad 2.20$$

The direction of the transmitted wave must be the same as that of the incident wave;

hence transmittance as a factor of both the transmitted and incident energy is written as:

$$\text{transmittance} = \frac{\text{transmitted energy}}{\text{incident energy}}$$

$$\frac{E_T}{E_1} = \frac{2n_0}{n_0 + n_1} \exp\left[ik_0 L \left(\frac{n_1}{n_0} - 1\right)\right] \quad 2.21$$

The heading of the reflected wave should be inverse to that of the occurrence wave;

hence reflectance as a factor of both the reflected and incident energy is written as:

$$\text{reflectance} = \frac{\text{reflected energy}}{\text{incident energy}}$$

$$\frac{E_R}{E_1} = \frac{n_0 - n_1}{n_0 + n_1} \exp(-2ik_0 L) \quad 2.22$$

The equation of reflectance is useful in the determination of the thickness of the anodized titanium samples while that of transmittance is used to determine the photocatalytic rate of the dye solution in the presence of the anodic titanium plate.

## 2.16 Dyes

Material colors utilized are unpredictable sweet-smelling natural mixes that are intended to oppose blurring upon openness to perspire, water, light, many oxidizing and diminishing synthetics, and furthermore microbial assault. Their applications in material businesses differ contingent upon the sort of textures (silk, rayon, cotton, fleece and so

on) produced. It has been accounted for that the overall market for colors is around  $7 \times 10^5$  tons for each year (Pearce et al, 2003). Shading and its force in colors is a result of the presence of chromophoric and auxochromic gatherings. Basically, chromophores are aryl gatherings, which contain delocalized ( $\pi$ ) electrons in the formed ring framework which are answerable for the retention of electromagnetic radiation of fluctuating frequencies, contingent upon the energy needed by the electron cloud. Notwithstanding the fundamental chromophore, color particles frequently contain auxochromes which contain electron pulling out or electron giving substituent bunches that adjust the general energy substance of the electron framework.

**Table 1: Characteristics of typical raw textile dyeing mill effluents (Pearce *et al*, 2003)**

<b>Parameters</b>	<b>Values</b>
pH	6-10
Temperature ( $^{\circ}\text{C}$ )	35-45
Biological Oxygen Demand ( $\text{mg L}^{-1}$ )	80-6000
Chemical Oxygen Demand ( $\text{mg L}^{-1}$ )	150-12000
Total Suspended Solids ( $\text{mg L}^{-1}$ )	15-8000
Total Dissolved Solids ( $\text{mg L}^{-1}$ )	2900-3100
Chlorine ( $\text{mg L}^{-1}$ )	1000-6000
Total Kjeldahl Nitrogen ( $\text{mg L}^{-1}$ )	70-80
Colour (Pt-Co units)	50-2500
Trace elements (Zn, Mn, Cu, Fe, B, F, $\text{PO}_4^{3-}$ , Cr, Ni, Hg, $\text{mg L}^{-1}$ )	< 10
Sulphate ( $\text{mg L}^{-1}$ )	600-1000
Oil and grease ( $\text{mg L}^{-1}$ )	10-30

The word auxochrome is gotten from two roots which are "auxo" and "chrome" signifying "expanded" and 'shading' separately. Along these lines, the importance of the word auxochrome is "shading power enhancer". Color particles accordingly contain auxochromes that are either emphatically or contrarily charged or their blends. The kinds of color of ionizable utilitarian gatherings that might be appended to auxochromes are: (a) -OH (hydroxyl) (b) -COOH (carboxyl) (c) -NH<sub>2</sub> (amino) and (d) -SO<sub>3</sub>H (sulphonic) attached to them (Chinta and VijayKumar, 2013).

The physico-compound properties and uses of material colors are remembered for Table 2. As per Colour Index (C. I), dyes may be classified as:

- a) Anionic which incorporates immediate, corrosive and receptive colors
- b) Cationic which incorporates essential colors and
- c) Non-ionic which incorporates scattered colors that don't ionize in fluid stage (Joshi *et al*, 2004).



**Table 2: Classes of dyes according to colour index (C.I.) (Wesenberg *et al*, 2003)**

<b>Code</b>	<b>Chemical Class</b>	<b>Code</b>	<b>Chemical Class</b>	<b>Code</b>	<b>Chemical Class</b>
10,000	Nitroso	42,000	Triarylmethane	53,000	Sulfur
10,300	Nitroso	45,000	Xanthene	55,000	Lactone
11,000	Monoazo	46,000	Acridine	56,000	Aminoketone
20,000	Disazo	47,000	Quinoline	57,000	Hydroxyketone
30,000	Trisazo	48,000	Methine	58,000	Anthraquinone
35,000	Polyazo	49,000	Thiazole	73,000	Indigoid
37,000	Azoic	49,400	Indamine	74,000	Phthalocyanine
40,000	Stilbene	50,000	Azine	75,000	Natural
40,800	Carotenoid	51,000	Oxazine	76,000	Oxidation Base
41,000	Diphenyl- methane	52,000	Thiazine	77,000	Inorganic

### 2.17 Concerns of textile dyeing effluents

Release of untreated material coloring effluents causes the accompanying natural issues (Foo and Hameed, 2010):

- a) Impart tone to the getting environment and make tasteful issue
- b) Limit the re-oxygenation limit of the accepting water and forestall transmission of daylight which thus upsets the photosynthetic exercises of benthic plants in the amphibian framework
- c) Persistent and intense poisonousness
- d) Cleavage of the azo linkage(s) in the colors under anaerobic conditions lead to the age of fragrant amines that are cancer-causing and mutagenic and
- e) In people, openness to colors and hued effluents may prompt immunological, neurological and circulatory issues, disturbance to lung edema, diseases of eye and skin and hypersensitivity issues.

The vast majority of the data identified with poisonousness of colors (for example cancer-causing nature, mutagenicity, mortality and genotoxicity) was gotten from tests utilizing creatures, for example, fish, rodents, green growth, microscopic organisms, protozoans and so forth (Sala and Gutierrez-Bouzan, 2012). Exploration indicated that algal photosynthesis and development were not repressed at color focus under 1 mg L<sup>-1</sup>, while then again, Novotny et al, (2006), detailed the inhibitory impacts of azo and anthraquinone colors on bacterial glow, algal development and reasonability, just as development and touching capacity of protozoan. From research, it is apparent that poisonousness of dyestuffs is reliant on its focus (Gümüs and Akbal, 2011).

## CHAPTER THREE

### METHODOLOGY

#### 3.1 Introduction

This chapter covers the experimental methods and procedures used to prepare TiO<sub>2</sub> films; the equipment's used to determine both the surface and optical measurements and the set up for photocatalytic measurement.

#### 3.2 Experimental methods

##### 3.2.1 Pretreatment of titanium substrate

The pretreatment processes varied from rinsing, degreasing and etching. Grade 1 titanium foil of 0.3 mm thickness was cut in rectangular pieces of 60 mm × 30 mm specimens, the sample was degreased in acetone solution for five minutes at ambient temperature after which etching (Acid activation) followed up.

Scratching was acted in an answer comprising of nitric corrosive, hydrofluoric corrosive and water in the proportion of 55:5:30 for five seconds. This cycle helps in eliminating the normal oxide layer appended to the outside of titanium metal as a result of its reaction with air. This process was followed by thorough cleaning of the titanium plate in distilled water.

##### 3.2.2 Anodic oxidation of Titanium (IV) Oxide films

The anodization equipment and apparatus used were;

- i. Philip Harris Hd power supply 0 – 350 Vdc 200 mA, 0 -35 Vac 200 mA. The power supply was used to anodize the sample at 200 Vdc.

- ii. Hot plate stirrer model L – 81. The stirrer was set at 800 revolution per minute (rpm) .
- iii. 0 – 100 °C thermometer. The thermometer was used to ensure a constant anodization current of 25 °C
- iv. CHY 40 R digital multimeter. The meter was used to measure the current generated during anodization at the intervals of 20 s.
- v. Measuring cylinder and electronic mass balance were used to accurately measure the reagents required.



**Figure 3.1: Experimental set up for anodization of TiO<sub>2</sub> plate. (Source : Author, 2018)**

A digital multimeter CHY 40 R was connected between the power supply and the anodising unit for the measurement of required voltage and current data collection.

The anodization set up comprises of the anodization cell (electrolytic cell), magnetic stirrer and water bath which regulates the temperature of the electrolyte, keeping it almost

constant. The distance of 1 cm between the anode and cathode was kept constant throughout the experiment by an electrode separator.

Anodization Procedure;

- i. The electrolyte consisted of 0.75 M  $\text{H}_2\text{SO}_4$ , 0.075% wt HF and distilled water at the ratio of 41:1:958.
- ii. The revolution speed of the magnetic stirrer was set at a constant rate of 800 rpm throughout the anodizing period.
- iii. Inter electrode spacing of 1cm was maintained between the anode and the cathode, while a 1:4 anode to cathode area ratio was made. Aluminium was used as the counter electrode.
- iv. Anodization was done at a constant voltage of 200 Vdc from 20 s to 30 min.
- v. Immediately after anodic oxidation, the samples were rinsed in distilled water thoroughly before drying in air and storing for pigmentation.

### **3.2.3 Pigmentation of Titanium plate**

The electro deposition cell was prepared with 0.1 M  $\text{CuSO}_4 \cdot 5\text{H}_2\text{O}$  electrolyte, and the pigmentation of the anodized plate was done at 12 Vdc for a period of 5 s. The anode was made of a copper plate placed at a distance of 1 cm from the titanium cathode plate. The pigmented sample and the set up are as shown in Figure 3.2.



**Figure 3.2: Electrodepositing set up for pigmentation. (Source: Author, 2018)**

### 3.2.4 Annealing of Titanium plates

Annealing was done by the use of a Muffle furnace for a period of four hours at a constant temperature of  $450\text{ }^{\circ}\text{C} \pm 5\text{ }^{\circ}\text{C}$ . The samples were placed inside Petri dishes, and then inserted into the furnace and the door locked tightly to avoid any contact with the outside environment as shown in Figure 3.3 (a) and (b).

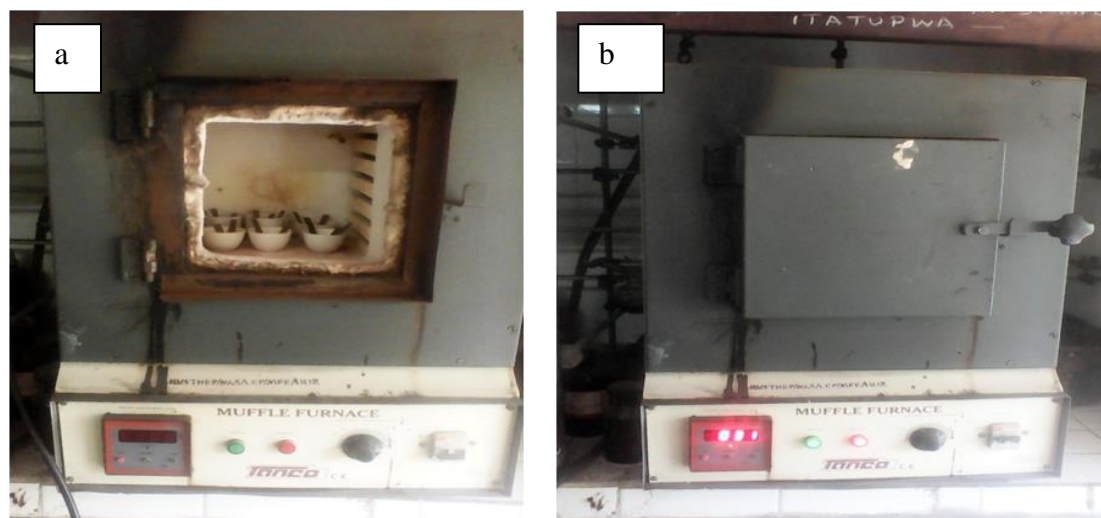


**Figure 3.3: Annealing furnace with (a) samples ready for heat treatment and (b) furnace set at  $450\text{ }^{\circ}\text{C}$  for 4 hrs with samples placed inside. (Source: Author, 2018)**

### 3.2.5 Spectral reflectance measurement

The type of spectrophotometer used to test the samples was Perkin Elmer (UV/VIS/NIR Lambda 9) Spectrometer. Reflectance of the samples was measured using an integrating sphere accessory. Sample was placed at the back of the sphere with the reference mirror placed at the reference sample holder point. The measurement of reflectance against wavelength was done in the range of  $250 \leq \lambda \leq 2500\text{nm}$  for all the samples.

Figure 3.4 shows a schematic diagram on how the total reflectance measurement takes place in an integrating sphere.

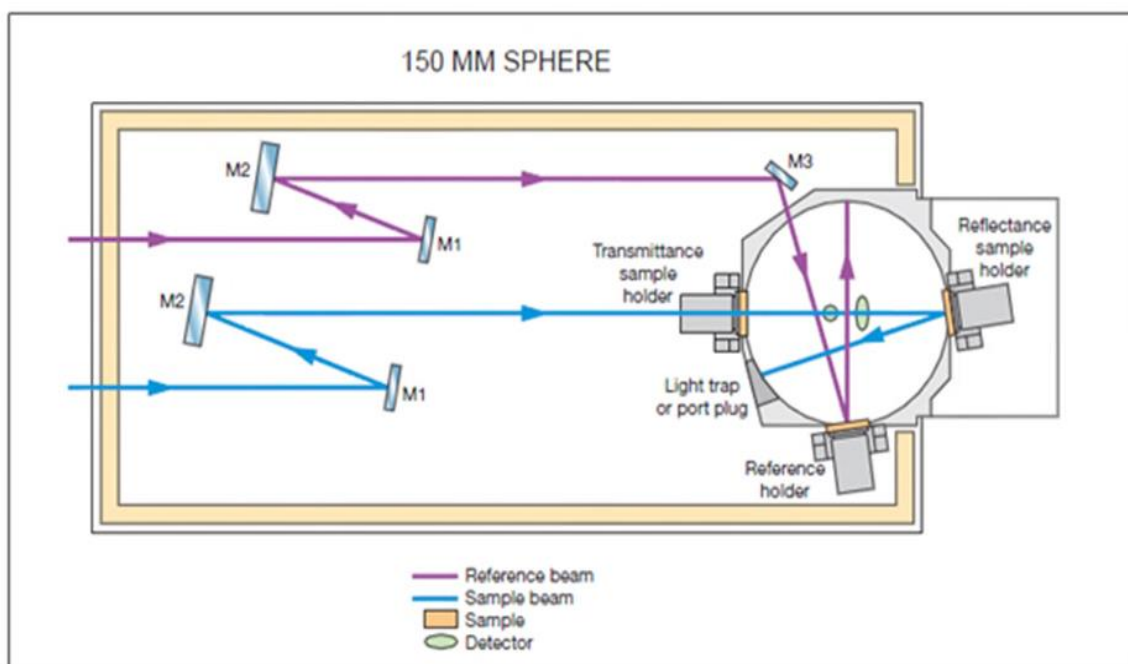


**Figure 3.4: Schematic diagram of reflectance measurement using integrating sphere.**  
(Source: Author, 2018)

Before the start of the measurement the following procedures were followed,

- i. The instrument was auto-zeroed with the barium sulfate mirrors at the reference and reflectance sample holder points.

- ii. The baseline correction measurement was done with the un-anodized sample placed at the reflectance sample holder point.
- iii. Measurements of the sample were done and the data recorded.

Figure 3.5 shows a photo of the Perkin Elmer (UV/VIS/NIR Lambda 9) Spectrometer.



**Figure 3.5: Perkin Elmer (UV/VIS/NIR Lambda 9) Photo-spectrometer set up with the Integrating Sphere accessory (Source: Author, 2018)**

### **3.2.6 Fourier-transform infrared spectroscopy (FTIR)**

The type of FTIR used to test the samples was Platinum FTR as shown in Figure 3.6. This technique is used to obtain infrared spectrum of absorption of  $\text{TiO}_2$  samples. The samples, starting with the un-anodized Ti were placed on the attenuated total reflectance (ATR) attachment and measurements done between the ranges of  $400 \text{ cm}^{-1} - 4000 \text{ cm}^{-1}$  wave number. The infrared light was used to scan test samples so as to determine the



chemical properties; the intensity was estimated as percent conveyance of the IR radiation as for the reference.

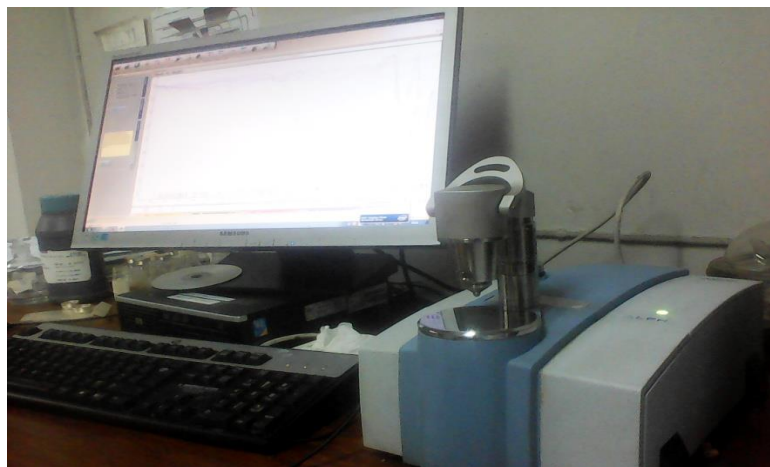


**Figure 3.6: Fourier transforms infra-red spectroscopy (Platinum FTR). (Source: Author, 2018)**

The computer processing software turns the raw data into the desired result by taking all the data and working backward to infer what the absorption should be at each wavelength.

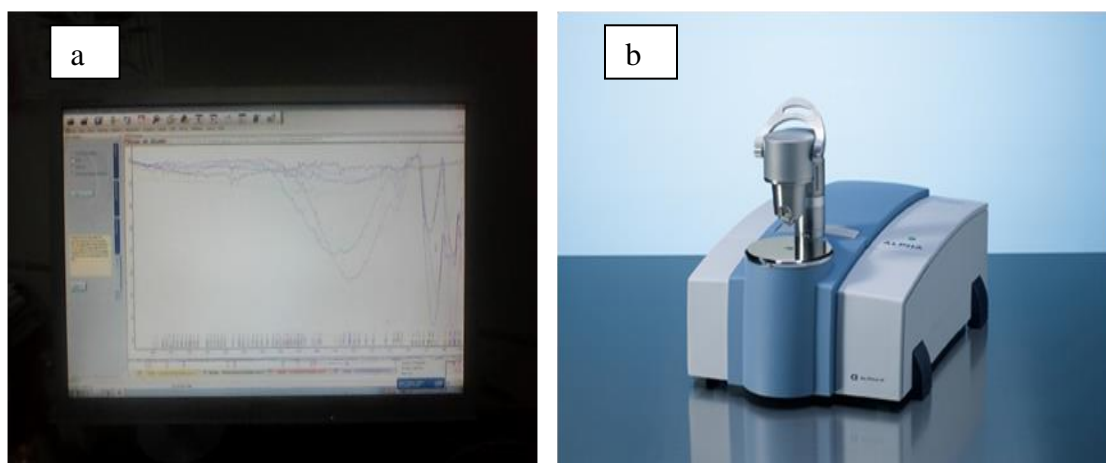


**Figure 3.7: (a) computer processing of raw data and (b) FTIR spectrometer with an attenuated total reflectance (ATR) attachment. (Source: Author, 2018)**

### 3.2.7 Atomic Force Microscopy (AFM)

The sort of AFM used to gauge the examples was NanoScopeIIIa Scanning test magnifying instrument regulator as found in Figure 3.8. The instrument was worked in tapping mode utilizing the RTESP7, 125  $\mu\text{m}$  pyramidal silicon tips with a resounding recurrence of 300 kHz. The example pictures were acquired at a sweep size and output paces of  $2 \times 2 \mu\text{m}$  and 1 Hz, separately. The AFM pictures acquired were utilized to decide the surface harshness of the examples.



**Figure 3.8: Atomic force microscopy set – up in operation. (Source: Author, 2018)**

The surface harshness of the examples is accomplished when the cantilever shaft with the assistance of a super fine needle connected to it goes through the edges and box of the example's surface. During this cycle, a laser shaft gleams on the avoided cantilever at a diagonal point; this permits direct estimation of the diversion in the cantilever by changing the laser pillars' point of rate. A picture is subsequently made indicating the

arrangements and the surface geology of the material under investigation.

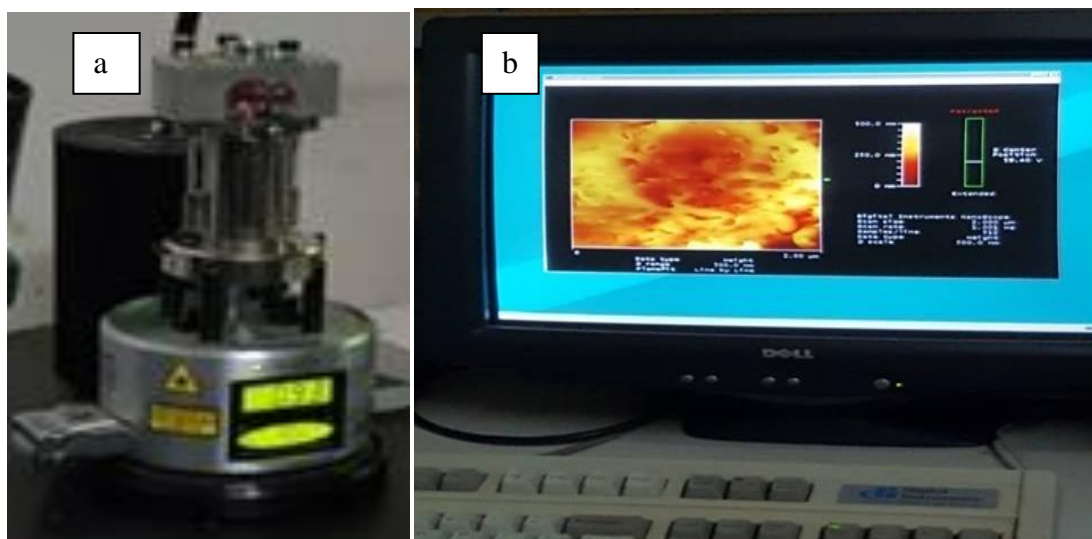


**Figure 3.9:** A photo of the (a) Atomic force microscope used in this study and (b) Image of the sample's morphology displayed by the monitor. (Source: Author, 2018)

The operating mode used to decide the surface geography of the examples was classified "tapping mode", on the grounds that the tip is tapped, the cantilever moves from the surface when the needle appended to it distinguishes a sharp valley or mountain, trying not to stall out because of direct contact with the surface. The surface images of the samples are as displayed on the computer screen as seen in Figure 3.9 (b)

### 3.2.8 Scanning Electron Microscopy (SEM)

Zeiss Crossbeam 540 FEG SEM was used to determine the surface morphology of the TiO<sub>2</sub> samples. SEM scanned images by using high energy beams of 20 kV on sample dimension of 1 cm × 1 cm of TiO<sub>2</sub> films anodized at different time intervals, pigmented and annealed at 450 °C for 4 hours so as to find out their surface morphology and composition. Surface topography of the material is detected when an electron beam of high energy is channeled through electromagnetic coils in a vacuum chamber which

focuses the electrons towards the atoms of the test sample. The collision with the surface of the sample generates an array of signals revealing the surface image (topography) of the sample.

These microscopes use up to 100 nA FIB current with exceptional spot profile to bridge the gap between micro and nanopatterning.

### **3.2.9 X – Ray diffractometer (XRD)**

The type of equipment used was German Bruker D2 Phaser X – beam diffractometer with a  $\text{CuK}\alpha$ . Radiation and frequency 0.15418 nm. The XRD estimation of  $2\theta$  examine were completed from  $20^\circ - 80^\circ$  with a sweep pace of  $2^\circ/\text{min}$  with proceeds with filter sort of 20 kV/200 mA through RINT 2000 vertical goniometer at fixed monochrometer. The occurrence point of the X-beam on the  $\text{TiO}_2$  test was looked over an enormous reach, the diffraction design relating to the useful obstruction tops from various precious stone planes were plotted to decide the gem stages, best direction of grains, stress, grain size and grid strain of the samples.

### **3.2.10 Photocatalysis.**

The photocatalytic performance was characterized by photodegradation of methylene blue using a photocatalytic reactor as shown in Figure 3.10. The reactor consists of a power supply, a base which has the electronic circuit that controls the entire reactor and a cuvette with a cover. The actual photocatalytic reaction takes place in the cuvette.



**Figure 3.10: Photocatalytic reactor equipment. (Source: Author, 2018)**

In a typical photocatalytic reactor, the electronic circuits operate the cooling motor, the UV light source, the magnetic stirrer, the source and detector of the light that goes through the cuvette.

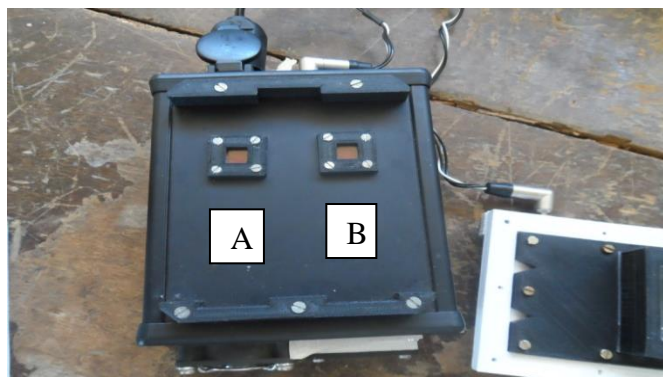


**Figure 3.11: Photocatalytic reactor base. (Source: Author, 2018)**

The base has two small windows, marked as A and B as shown in Figure 3.11, which allow light to pass into the cuvette (photoreaction unit) and out of the cuvette to a detector in the base which measures the intensity of the light. This set up determines the light absorbed by the substance in the cuvette. The photoreaction unit is placed on top of the base where it receives magnetism from the magnetic stirrer and light for determining the concentration of the sample under test.

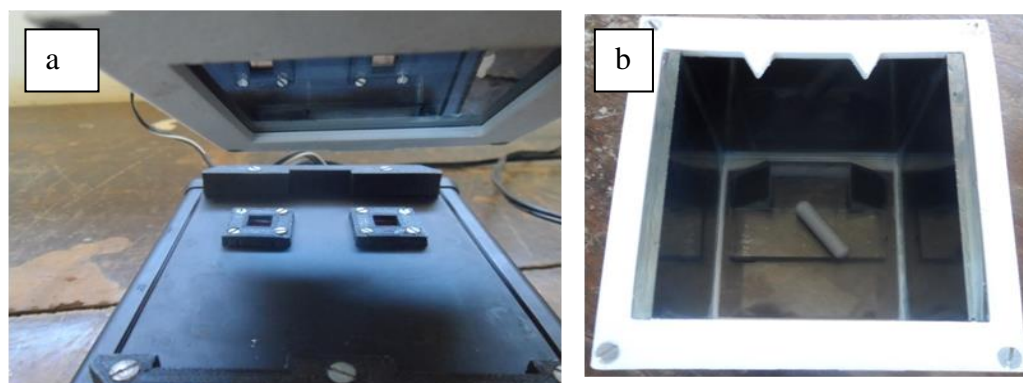


**Figure 3.12: (a) photoreaction unit and (b) top view of photoreaction unit cuvette. (Source: Author, 2018)**

The photoreaction unit has a stirrer, two 45° rectangular prisms and highly reflective walls. The bottom of the photoreaction unit is transparent so as to allow light to enter the chamber.



**Figure 3.13: Inside of photoreaction unit cuvette. (Source: Author, 2018)**

The cover of the photoreaction unit has a UV source controlled automatically, while its top has a Motor which runs a cooling fan for the UV source.

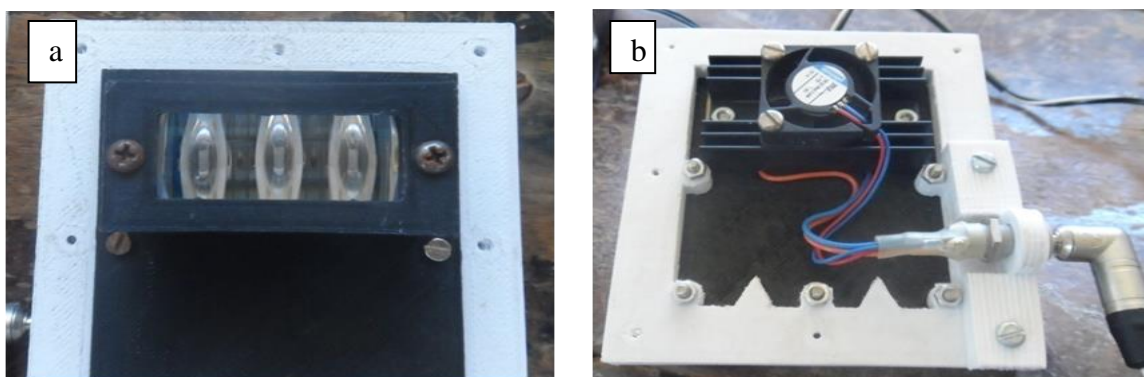


**Figure 3.14: (a) UV source and (b) UV source cooling fan. (Source: Author, 2018)**

Each sample piece measuring 60 mm × 30 mm was placed in a photocatalytic reactor with 100 ml 1 ppm methylene blue solution at its natural pH for photocatalysis. Lutron UV-340 UV light meter measuring between 290 nm and 390 nm of electromagnetic radiation was used.





**Figure 3.15: Lutron UV-340 UV light meter. (Source: Author, 2018)**

The photocatalytic measurements were carried out between 12:30 noon and 1:30 pm daily for a period of one month repeatedly when the skies were clear. The data was recorded for 20 min in dark phase followed by 40 min in the presence of sunlight. The reactor collected data after every 2 min automatically on a laptop which was then analyzed as seen in Figure 3.16 (b). Prior to solar UV irradiation, the solution was kept under dark condition (dark phase) for 20 min to allow for adsorption to equilibrate. During the dark phase there was continuous stirring.

A control experiment was performed without the samples to estimate the rate of photolysis and adsorption over the period of time that the photocatalytic degradation by the samples was to be performed.



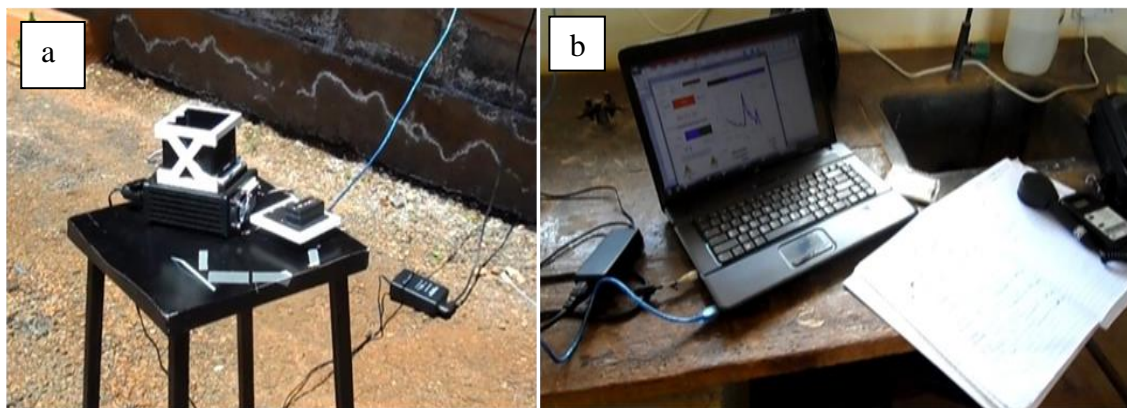


**Figure 3.16: (a) reactor in the sun and (b) Photocatalytic data acquisition unit. (Source: Author, 2018)**

## CHAPTER FOUR

### RESULTS AND DISCUSSION

#### 4.1 Introduction

This chapter presents the structural and optical properties of anodic TiO<sub>2</sub> samples that were prepared and the findings discussed. The primary reason for this investigation is to establish the optimum anodization time of the films that better photodegrades dye in water. This was done using a photocatalytic reactor shown in chapter four.

#### 4.2 Effect of anodizing time on color formation of the oxide films

Anodized titanium samples displayed different colors for different anodization times. Figure 4.1 shows the samples anodized at a consistent voltage of 200 V for a time of between 20 s and 120 s. The adjustment in shading shows a slim oxide film of shifting thickness shaped on the outside of the example reliant on the span of anodization. The variety of shadings framed on the anodic oxide movies can be clarified utilizing the different shaft obstruction hypothesis (Edwards, 1997).

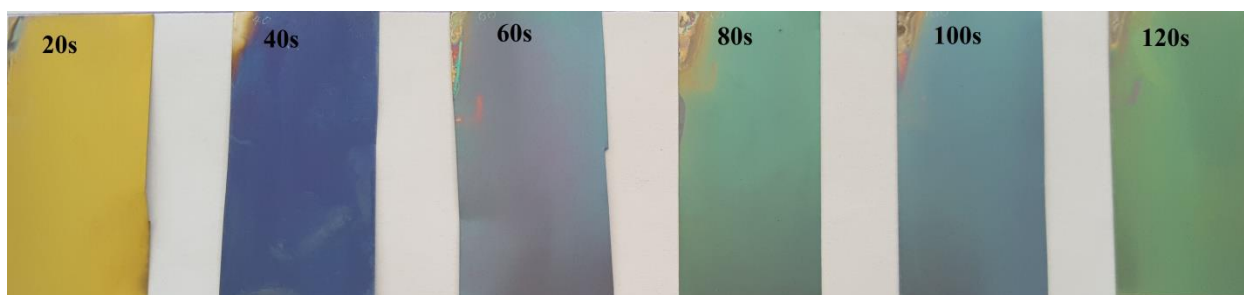


**Figure 4.1: TiO<sub>2</sub> samples anodized between 20 s and 120 s.**

These colors are not formed by absorption of certain wavelengths in the visible spectrum but by interference of the light reflected at the air-oxide interface and the light reflected at the metal substrate-oxide interface.

Figure 4.2 shows the coloration effects for samples anodized at different time intervals. Samples anodized between 3min to 8 min exhibited only slight change in color, however as the anodization time was prolonged; there was no significant change in color. The sample anodized for 10 min showed an occurrence of tiny grain-like structures whose size increased and became more enlarged as the anodization time was prolonged to 30 min. This is a clear indication that there is indeed a formation of pores on the oxide layer of  $\text{TiO}_2$  surface.

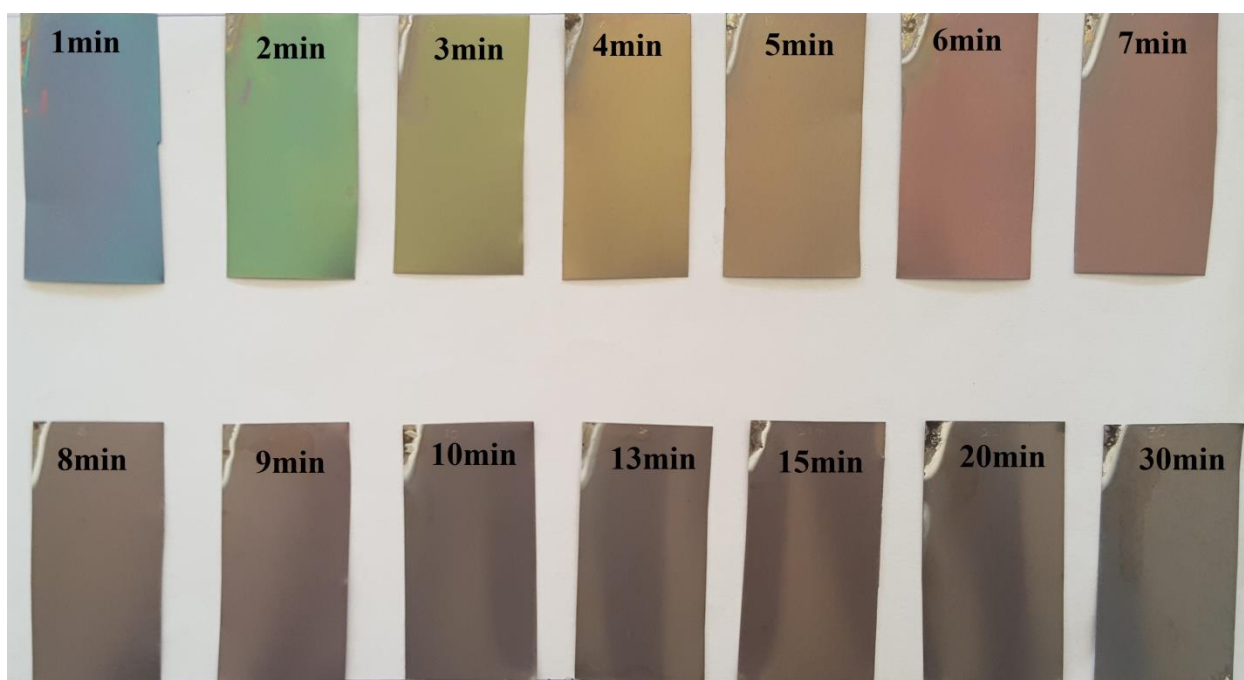


**Figure 4.2:  $\text{TiO}_2$  samples anodized from 1 min to 30 min**

Liang Wu et al, (2014) reported that the production of  $\text{O}_2$  bubbles during anodization is liable for the formation of both the porous surface morphology and cracks in the Ti films.

### 4.3 Effect of anodization time on current

The duration of anodization plays a significant part in the formation of an oxide layer on the surface of the sample. This is demonstrated by a pattern that presents itself as the samples undergo anodization at different time intervals. The current measurements were taken after every 20 s from the beginning of anodization and the pattern plotted as seen in Figure 4.3. The figure shows a drastic drop of current from the start of anodization to around 3 min which relates to the change in color as seen in Figures 4.1 and 4.2. Previous studies have reported that the current drop during anodization is due to the development of an oxide layer on the Ti surface (Regonini *et al*, 2013). It's further recorded that the interference colors are affected by the thickness of anodic oxide films where the change in color represents a new oxide layer formed on the Ti surface (Liang *et al*, 2014). It's therefore clear that, the drastic drop in anodization current is because of the arrangement of an oxide layer of differing thickness on the Ti test. Figures 4.2 and 4.3 shows that as the anodization current settles, there is no huge change in shading, and this is ascribed to the pace of development of the oxide layer on the oxide/metal interface to the pace of disintegration of a similar oxide layer at the lower part of the electrolyte which are in harmony (Regonini *et al*, 2013). It tends to be presumed that the example of anodization current as a component of time directly affects the adjustment in shading and the development of an oxide layer of shifting thickness on the outside of the samples. This is confirmed by the different colors attained during anodization.

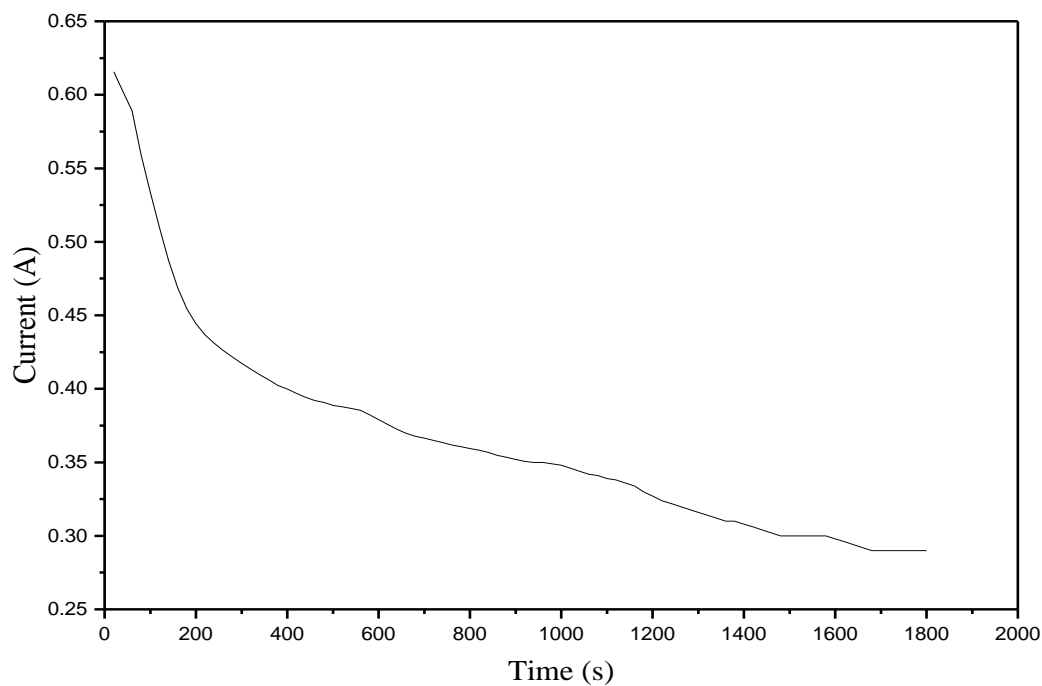


**Figure 4.3: Effect of anodization time on the current pattern**

#### **4.4 Optical properties of anodic TiO<sub>2</sub> films**

##### **4.4.1 Reflectance measurement of anodic TiO<sub>2</sub> films**

The crystal structure, as well as the surface and chemical state of a material assumes a significant role in the determination of its reflectance properties. The spectral reflectance of TiO<sub>2</sub> thin film was recorded in the range  $250 \text{ nm} \leq \lambda \leq 2500 \text{ nm}$ . The spectral reflectance spectra of the films anodized at different time intervals are shown in Figure 4.4.

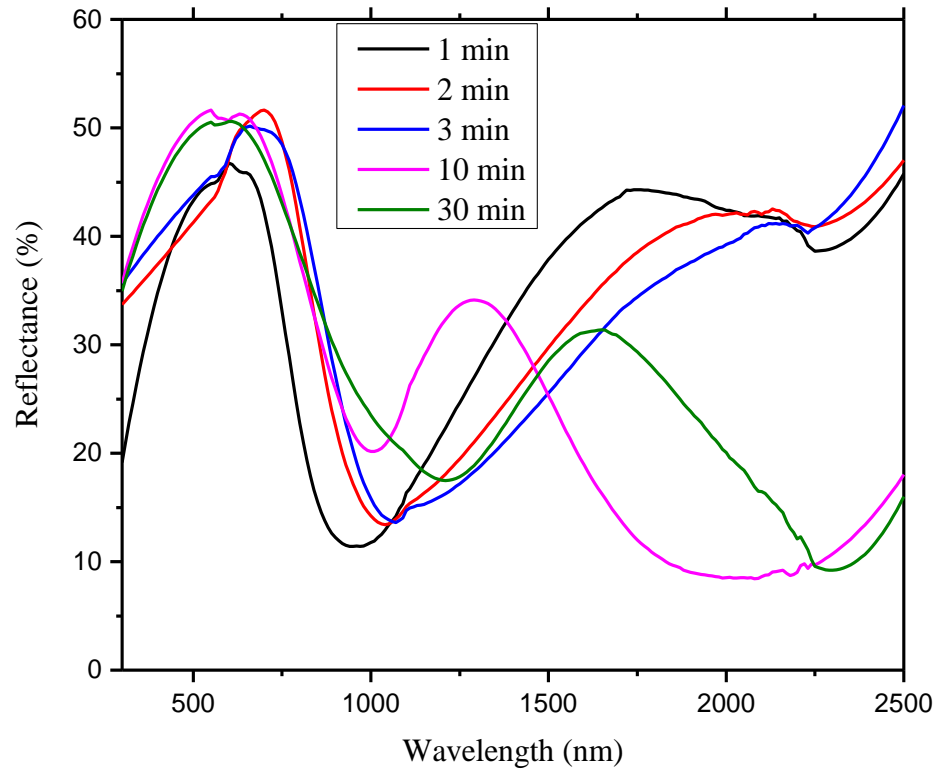


**Figure 4.4: Reflection spectra of anodic TiO<sub>2</sub> thin films as a function of wavelength.**

The thicknesses of the samples were determined using the wavelength at maximum percentage where the spectral reflectance occurred. Equations 4.1 and 4.2 were applied to calculate the film's refractive index and the thickness of the samples respectively.

$$n^2 = 5.193 + \frac{2.441 \times 10^7}{\lambda_{max}^2 - 0.803 \times 10^7} \quad 4.1$$

In this equation  $n$  is the refractive index of the sample and  $\lambda_{max}$  is the wavelength at a maximum percentage of the wave. Using equation 4.1, the refractive indices of the samples anodized at different time intervals were obtained and these are shown in Table 3. There was a slight decrease of refractive index for samples anodized in 1 min to 2 min.

The sample anodized at 10 min showed a higher value of refractive index while the sample anodized at 2 min had the lowest value of approximately 2.4.

After obtaining the refractive indices, equation 4.2 was used to determine the thickness of the samples.

$$t = \frac{\lambda_{\max}}{4n} \quad 4.2$$

In equation 4.2,  $t$  is the thickness of the oxide layer formed on the sample,  $\lambda_{\max}$  is the wavelength at maximum percentage of the wave,  $n$  is the film's refractive index. From Table 3, it can be observed that the thickness of the samples increased from 105 nm for sample anodized for 1 min to 125 nm for sample anodized for 2 min. Thereafter, the thickness decreased to 96 nm for sample anodized for 10 min before increasing up to 117 nm for sample anodized for 30 min. These outcomes are like those saw by Allam et al, (2008) who detailed that as the anodization time draws out, because of field-improved oxidation, field-helped oxide disintegration, just as compound disintegration, the interface of Ti/oxide slowly moves further into the Ti metal and the external surface (oxide layer) breaks up into the arrangement. The presence of hydrofluoric corrosive (HF) in the electrolyte likewise assumes a significant part in quickening the pace of disintegration by burning-through titanium particles in the arrangement (Gong et al, 2001). This finding clarifies the explanations for the decline of oxide layer thickness as the anodization time approaches 10 min with a special case for the example anodized for 30 min where there seems both an expansion of the oxide layer and disintegration of a similar oxide layer on various pieces of the example. The sample anodized for 2 min therefore exhibited the highest thickness as seen in Table 3.

**Table 3 Variation of TiO<sub>2</sub> film thickness with anodization time**

Anodization time (min)	Refractive index	TiO <sub>2</sub> film thickness (nm)
1	2.4179	105.79
2	2.3984	125.14
3	2.4161	107.69
10	2.4262	96.41
30	2.4211	117.3

#### 4.4.2 Fourier-transform infrared (FTIR) spectroscopy measurement

The FTIR sketch has two group regions. The functional group region which runs from 4000 cm<sup>-1</sup> to 1450 cm<sup>-1</sup>, and the fingerprint region which runs from 1450 cm<sup>-1</sup> to 400 cm<sup>-1</sup>. Figure 4.5 show that pure titanium plate has less than 3% transmittance in the infrared region of the spectrum and it can therefore be said to be opaque. For the anodized TiO<sub>2</sub> samples, the FTIR spectra show slight shifts in absorption bands which are not seen in the spectrum for the pure sample as seen in Figure 4.6.



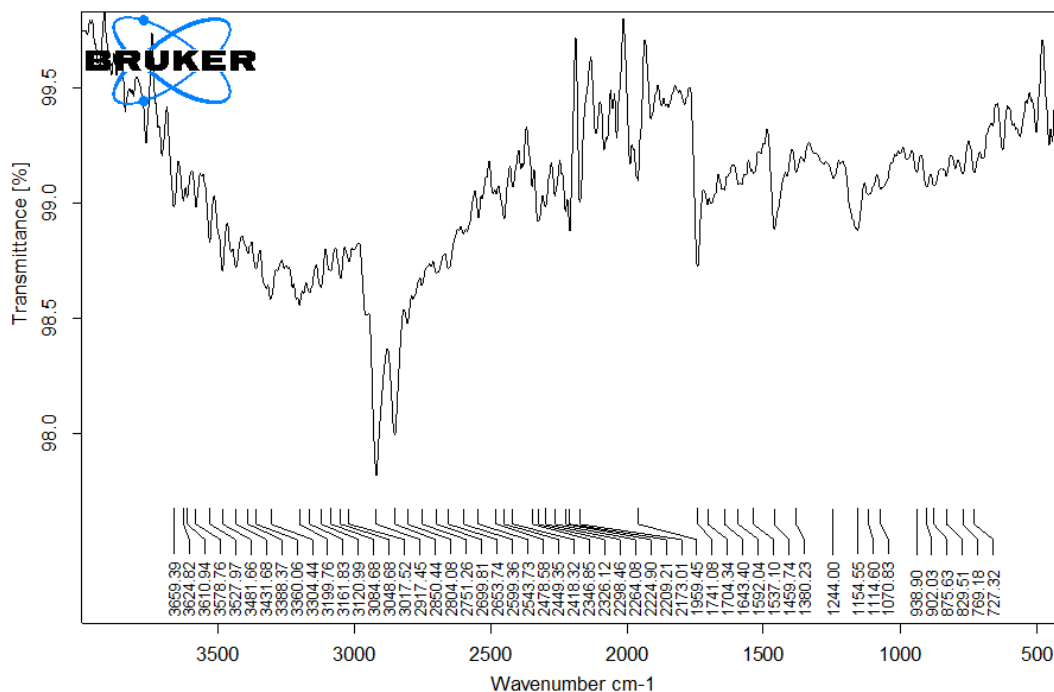


**Figure 4.5: FTIR spectrum of pure titanium**

Figure 4.6 shows the FTIR measurement of  $\text{TiO}_2$  anodized at different time intervals. From the Figure, the functional group region of the spectra shows that the samples anodized at different time intervals contain relatively few peaks; these are typically associated with the stretching, bending and twisting of covalent bonds in functional groups present in a sample upon the exposure to IR radiation. The samples anodized for a duration of 10 min and 30 min showed broad intensity peaks/features in this region which overlapped to the fingerprint region with peaks at  $1610 \text{ cm}^{-1}$  and  $1670.3 \text{ cm}^{-1}$  respectively. This is because of the presence of twisting vibration mode of the OH functional group which is related to water molecules appended to the surface of  $\text{TiO}_2$  (SharmilaDevi *et al*, 2014).

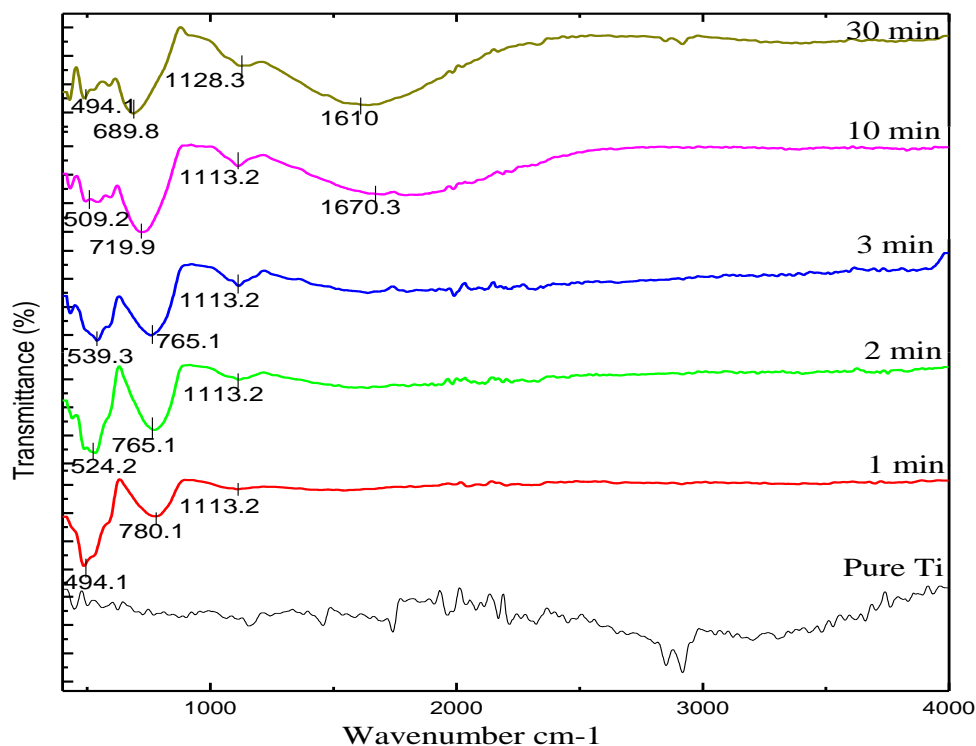


**Figure 4.6: FTIR spectra of TiO<sub>2</sub> anodized at different time intervals**

In the fingerprint region, the spectra contain data about the substance structure and actual condition of the material under examination. Tops in this area arise generally from complex twisting of the particle. They may be ordinary for sub-atomic evenness, or mix groups emerging from numerous bonds distorting all the while. In this region, samples anodized for 1 min, 2 min, 3 min, 10 min and 30 min exhibited peaks at  $494.1\text{ cm}^{-1}$ ,  $524.2\text{ cm}^{-1}$ ,  $539.3\text{ cm}^{-1}$ ,  $509.2\text{ cm}^{-1}$  and  $494.1\text{ cm}^{-1}$  respectively which can be assigned to Ti – O - Ti vibrations, (Arconada *et al*, 2009). They also exhibited peaks at  $780.1\text{ cm}^{-1}$ ,  $765.1\text{ cm}^{-1}$ ,  $765.1\text{ cm}^{-1}$   $719.9\text{ cm}^{-1}$  and  $689.8\text{ cm}^{-1}$  respectively, which are due to Ti = O bending vibration modes in the anatase morphology of titania as observed by various researchers (Bagheri *et al*, 2014 and Trivedi *et al*, 2015). A closer look at Figure 4.6 shows the

intensity of the peaks representing Ti – O - Ti vibrations decreases with the increase of anodization time, while those representing Ti = O bending vibration mode tends to increase. This implies a change in the chemical composition and surface morphology of the samples as the anodization time is increased. These samples also showed a weak peak at  $1128.2\text{ cm}^{-1}$ , which indicates the presence of sulfone ions coordinated to the metal cation  $\text{Ti}^{4+}$ . These peaks become more pronounced as the anodization time prolongs thereby becoming part of a wider spectrum into the functional group region. It has been reported that, metallic oxides altered with sulfate particles and further thermally treated at  $400\text{ }^{\circ}\text{C}$  show a band close to  $1140 \pm 20$  and between  $1390\text{ cm}^{-1}$  -  $1370\text{ cm}^{-1}$  that relates to an extending vibration mode brought about by S = O bonds (Sohn *et al*, 2004).

#### 4.4.3 X-ray diffraction measurement

Figure 4.7 shows a typical XRD pattern of  $\text{TiO}_2$  film anodized at different time intervals, pigmented and annealed for a period of four hours at a constant temperature of  $450\text{ }^{\circ}\text{C} \pm 5\text{ }^{\circ}\text{C}$  for. The samples had diffraction peaks at  $2\theta$  values of  $27.9^{\circ}$ ,  $37.0^{\circ}$ ,  $61.81^{\circ}$  and  $69.5^{\circ}$ , that can be readily attributed to (110), (101), (002) and (112) planes which correspond to a tetragonal crystal structure of rutile phase, the peak at  $61.81^{\circ}$  also identifies the presence of CuO coordinated to the metal cation  $\text{Ti}^{4+}$ . The diffraction peaks at  $38.8^{\circ}$ ,  $51.75^{\circ}$  and  $75.1^{\circ}$  can be attributed to (004), (105) and (215) planes of anatase  $\text{TiO}_2$ . This confirms the coexistence of both rutile  $\text{TiO}_2$  and anatase  $\text{TiO}_2$  phases in the annealed samples.

The intensity of the (101) peak is the strongest in all peaks corresponding to rutile phase which indicates that the growth of  $\text{TiO}_2$  is highly oriented along the (101) plane.

Diffraction peaks (110) and (004) grew in intensity compared to the unanodized TiO<sub>2</sub> sample with peak (110) being more intense at anodization time of 1 min.

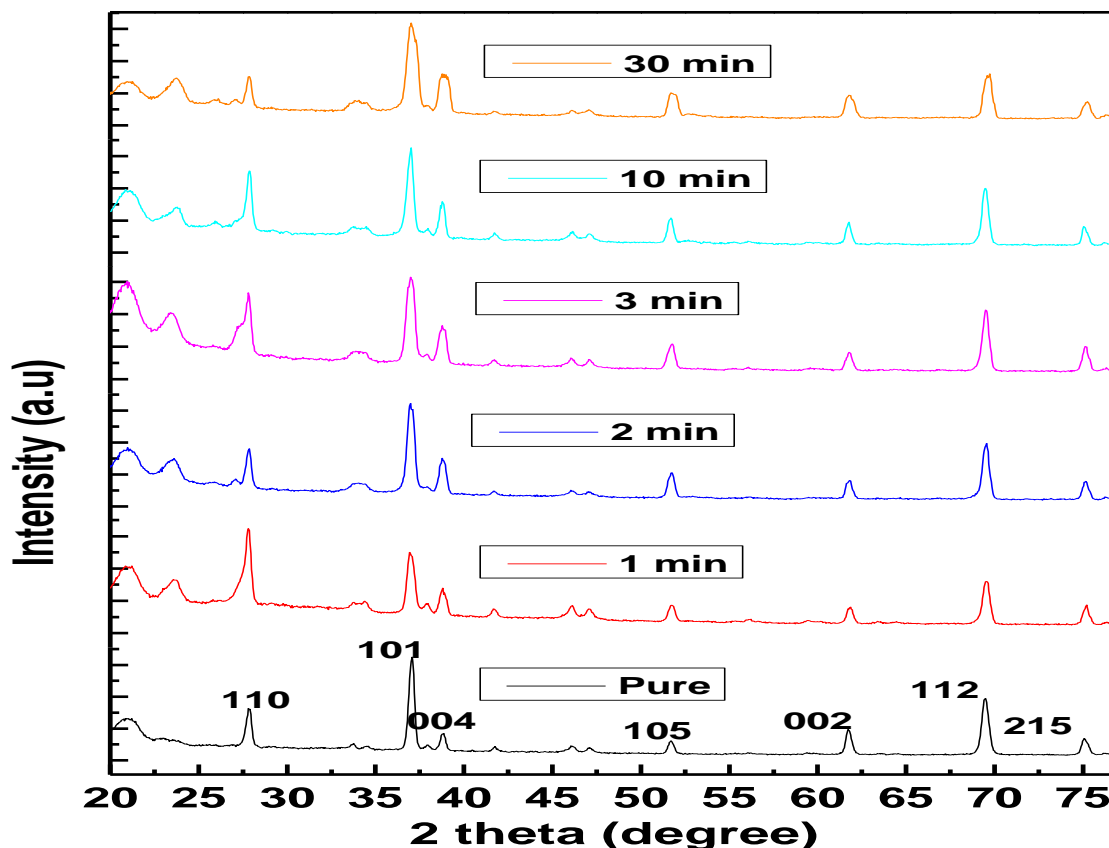


Figure 4.7: XRD patterns of TiO<sub>2</sub> films anodized for different time intervals.

The mean crystallite size of TiO<sub>2</sub> films was calculated using the Scherrer's formula

$$D = \frac{K\lambda}{\beta \cos\theta} \quad 4.3$$

Where, D is the normal crystallite size,  $\lambda$  is the X-beam frequency,  $\beta$  is the full width at half greatest (FWHM) of the predominant pinnacle and  $\theta$  is the Bragg point. The pure unanodized TiO<sub>2</sub> film exhibited a crystallite size of 0.37 nm which was higher than the anodized ones. At 1 min, 2 min, 3 min, 10 min and 30 min the crystallite size were 0.19 nm, 0.22 nm, 0.25 nm, 0.26 nm and 0.18 nm respectively. This trend shows an increase in

the crystallite size from 1 min of anodization then a significant decrease towards anodization time of 30 min.

The dislocation density was calculated using the relations

$$\delta = \frac{1}{D^2} \quad 4.4$$

Using this expression, the disengagement thickness was found to diminish with increment in anodization time which suggests a reduction in grid defect because of the expansion in crystallite size. The only exception was at anodization time of 30 min where the dislocation density was found to increase.

The micro strain was calculated using the relations

$$\varepsilon = \frac{\beta \cos \theta}{4} \quad 4.5$$

This study revealed that the strain got lower with increasing anodization time but increases at 30 min.

**Table 4: Effect of anodization time on the average crystallite size (D), dislocation density ( $\delta$ ) and micro strain ( $\epsilon$ ) of various TiO<sub>2</sub> samples**

Anodization Time	Average Crystallite size (D)	Dislocation Density ( $\delta$ )	Micro Strain ( $\epsilon$ )
1 min	0.19	27.7	0.186
2 min	0.22	20.7	0.166
3 min	0.25	16.0	0.142
10 min	0.26	14.8	0.139
30 min	0.18	30.9	0.199

## 4.5 Surface characteristics of TiO<sub>2</sub> films

### 4.5.1 Atomic Force Microscopy (AFM)

The AFM images revealed distinct topography for all samples. The morphology and distribution of the pores were found to be affected by the duration of anodization. The AFM images of the un-anodized Ti sample and those anodized at different time intervals of 1 min, 2 min, 3 min, 10 min and 30 min are as shown in Figure 4.8.

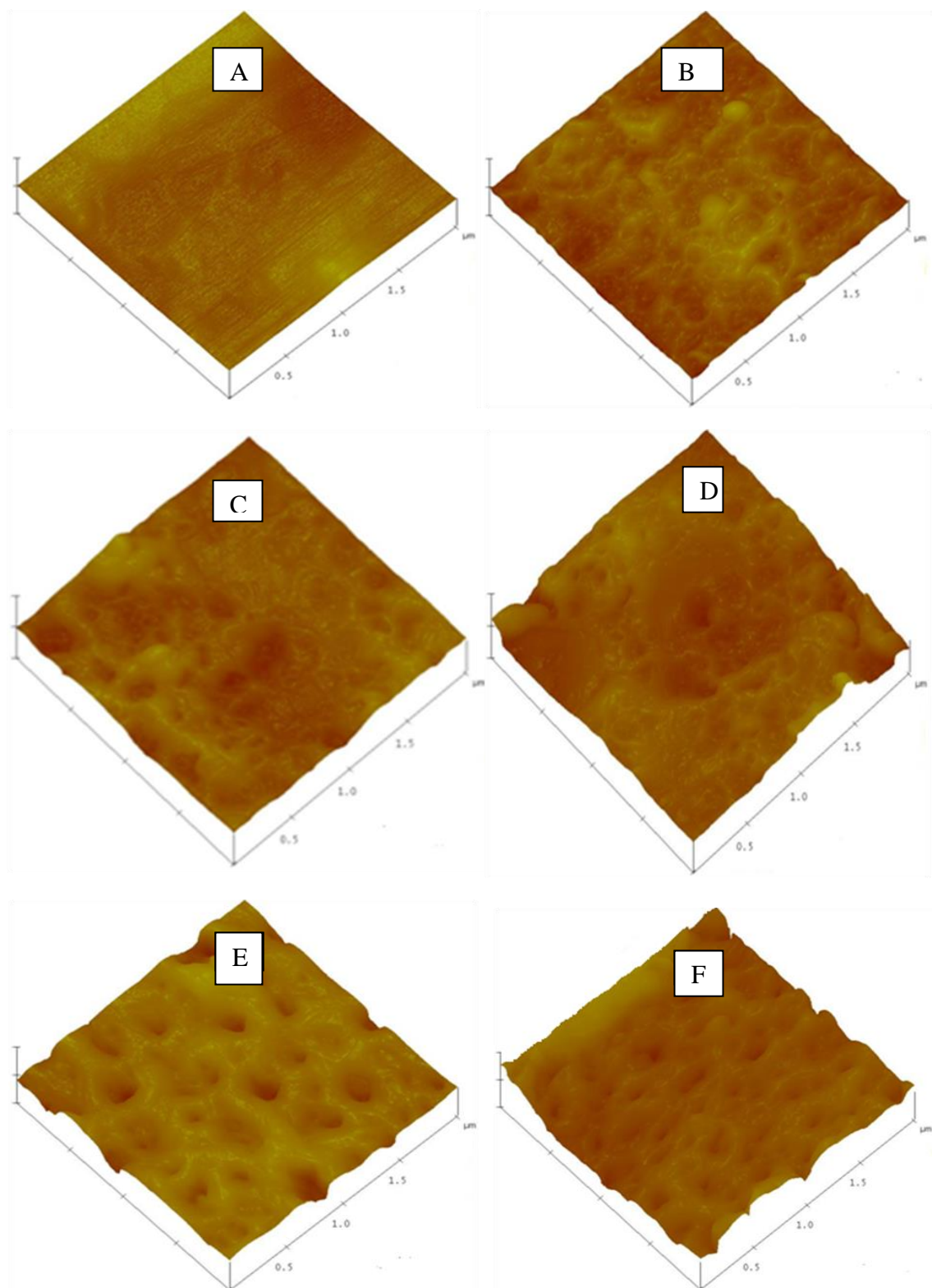


**Figure 4.8: Atomic Force Microscopy (AFM) showing the effect of anodization time on the morphology of the samples, (A) un-nodized Ti (B) 1 minute (C) 2 minutes (D) 3 minutes (E) 10 minutes and (F) 30 minutes**

Before anodization, the surface of metallic titanium sample was smooth and homogeneous as seen in Figure 4.8 A. Figures 4.8 B, C and D shows that in the initial stages of anodization, there is uneven distribution of the oxide layer on the Ti samples with a low surface roughness. For longer anodization time, the formation of pores becomes more pronounced and unevenly distributed. Each sample scanned at different positions exhibited the same topography but with a slight shift in the surface features. The Ti sample anodized for 30 min exhibited unique features as shown in Figure 4.9. The image shows an inhomogeneous distribution of surface features with a continuous oxidation of the surface on some parts of the sample but not on other parts. This finding can be explained based on the three cycles to be specific, field-upgraded oxidation of titanium foil, field-helped oxide disintegration, and synthetic oxide disintegration (Quan *et al*, 2005).

oxidation prompting the development of an oxide layer on the metals' surface, as the oxygen particles in the electrolyte arrangement move towards the interface of the metal and the oxide layer. During field-helped oxide disintegration, the oxide layer breaks down into the electrolyte because of the development of titanium particles from the metal-oxide interface through the oxide layer into the arrangement. The presence of hydrofluoric corrosive (HF) in the electrolyte helps in quickening the pace of disintegration of the oxide layer by devouring titanium particles in the arrangement (Gong *et al*, 2001). Increasing the anodization time promotes the formation of pores on the TiO<sub>2</sub> film as seen in Figure 4.9.



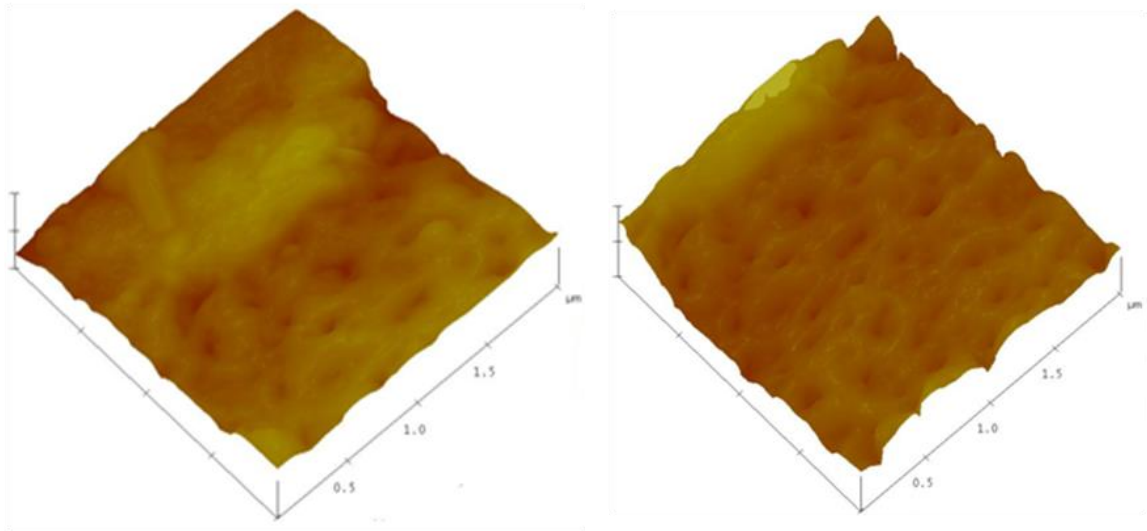


**Figure 4.9: Surface morphology of sample taken at different positions and anodized for 30 min**

#### **4.5.2 Surface roughness**

Surface unpleasantness is a significant quality of the oxide film and essentially influences its properties. To examine the impact of anodization on a superficial level harshness of the oxide film, the normal surface unpleasantness (Ra) and root mean square of the example harshness (Rms) were acquired by permitting the product to look over changed areas of two-dimensional AFM tests' morphology. It very well may be seen from Figure 4.10 that the Ra and Rms of the oxide film on the surface of the sample anodized for 1 min, 2 min, 3 min 10 min and 30 min are 18.87 and 24.63, 21.46 and 33.04, 39.17 and 51.27, 40.95 and 55.71, 77.08 and 90.81, respectively, which indicates that the roughness of the oxide film increased with the increase of anodization time.

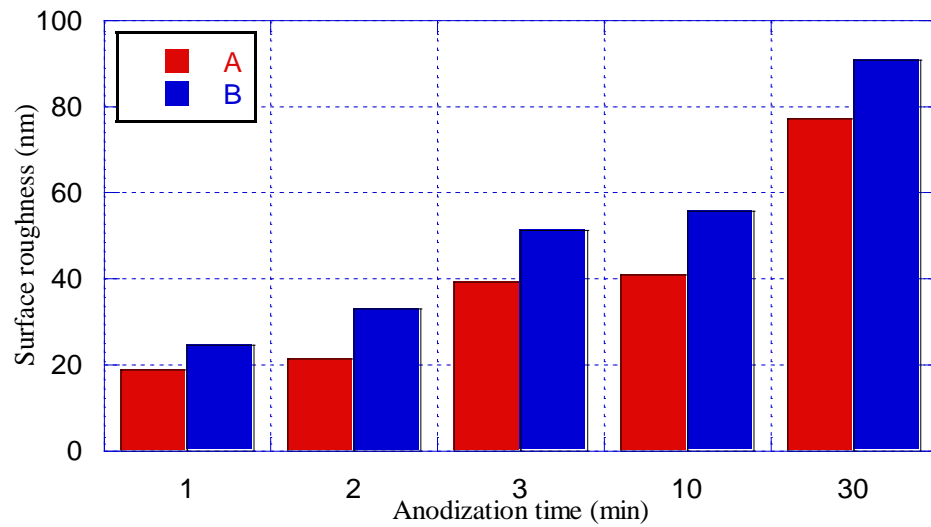


**Figure 4.10: Comparison of sample's surface roughness against anodizing time (a) the average surface roughness (Ra) and (b) root mean square of the sample roughness (Rms)**

Figure 4.11 shows the section analysis of the anodized samples giving a picture of the surface roughness as the anodization time is prolonged. The section analysis shows that un-anodized samples are almost smooth but with some degree of roughness. As the anodization time is prolonged the surface roughness increases.

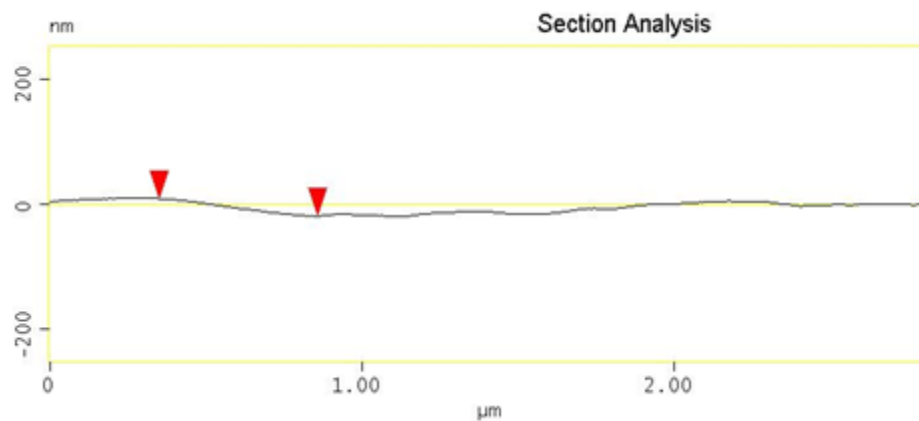


**Figure 4.11 (a): Surface cross-section of un-anodized Ti sample**

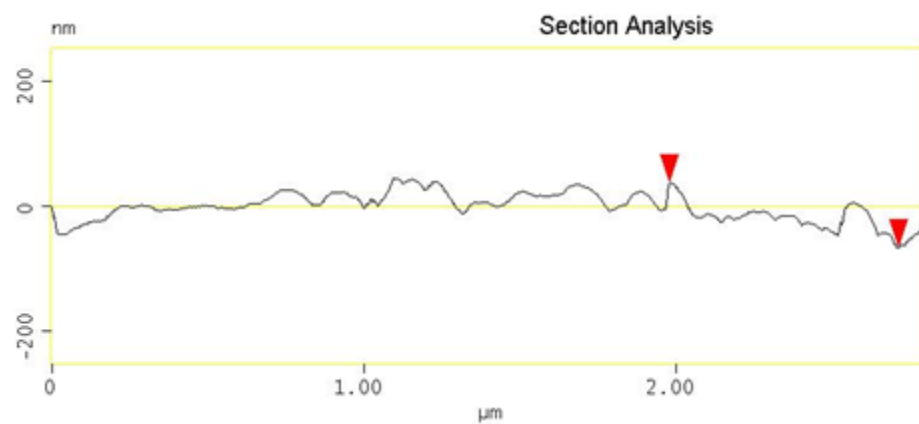


**Figure 4.11 (b): Surface cross-section of  $\text{TiO}_2$  film anodized for 1 min.**

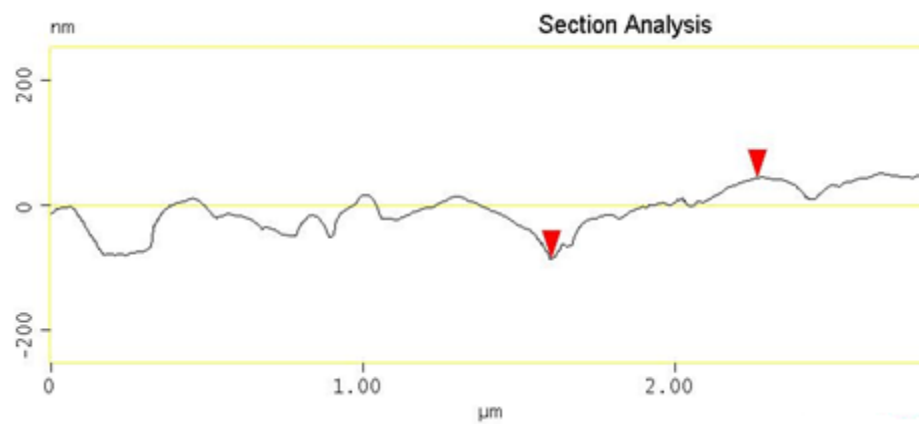


**Figure 4.11 (c): Surface cross-section of  $\text{TiO}_2$  film anodized for 2 min.**

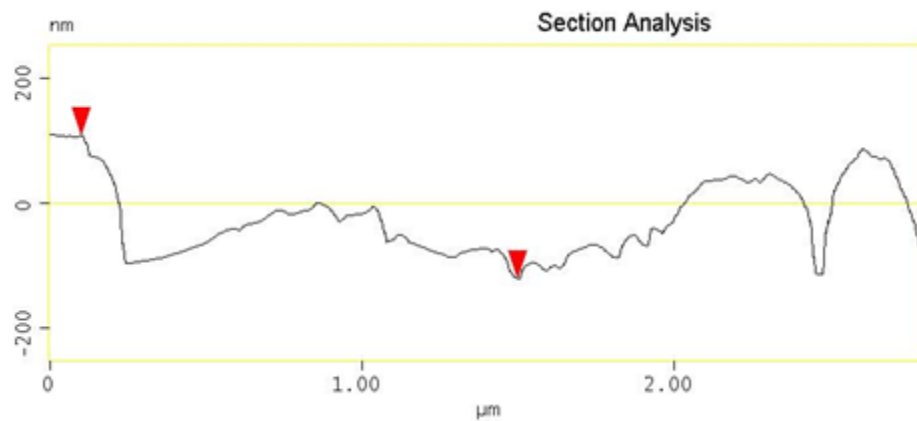


**Figure 4.11 (d): Surface cross-section of TiO<sub>2</sub> film anodized for 3 min.**

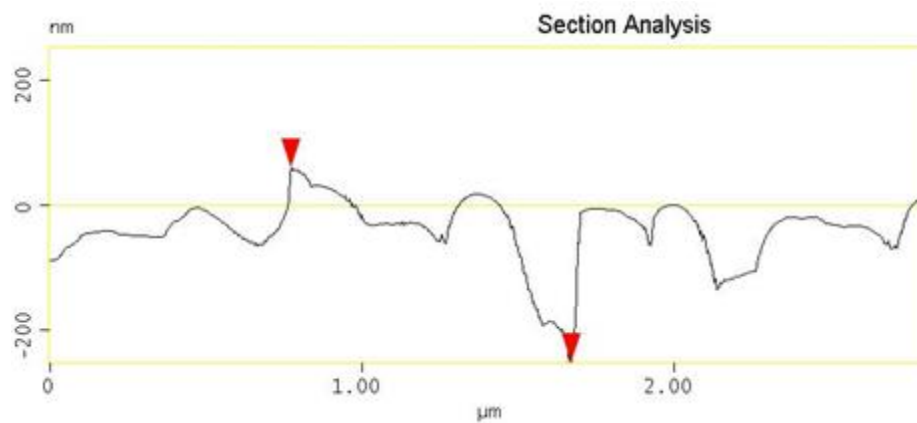


**Figure 4.11 (e): Surface cross-section of TiO<sub>2</sub> film anodized for 10 min.**

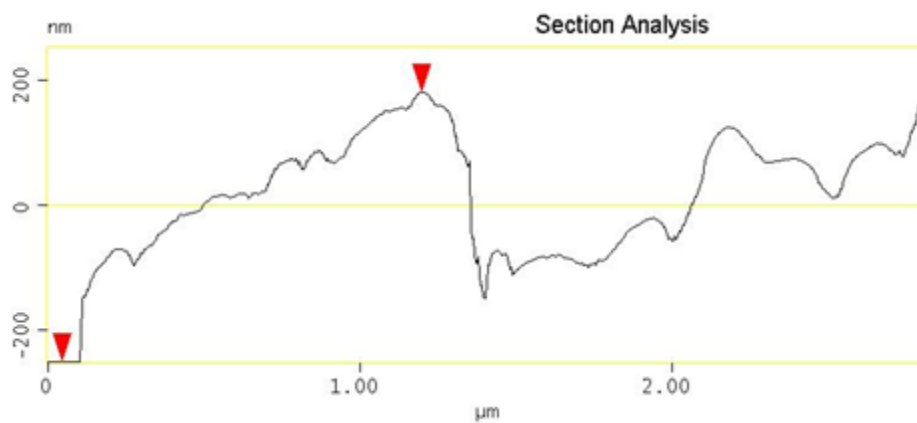


**Figure 4.11 (f): Surface cross-section of TiO<sub>2</sub> film anodized for 30 min.**

The oxide layer seems to have uneven distribution on the surface of the samples anodized at lower time intervals. Continual anodization for longer time increases the surface roughness and creates deeper pores which provide reaction sites for photocatalysis.

### **4.5.3 Scanning Electron Microscopy (SEM)**

Figure 4.12 shows SEM images for samples anodized at 200 V for different time intervals of 1 min, 2 min, 3 min, 10 min and 30 min and then pigmented and annealed at  $450\text{ }^{\circ}\text{C} \pm 5\text{ }^{\circ}\text{C}$  for 4 hours. It is clear that the structure and morphology of the oxide layers on Ti samples changes when the duration of anodization is prolonged.

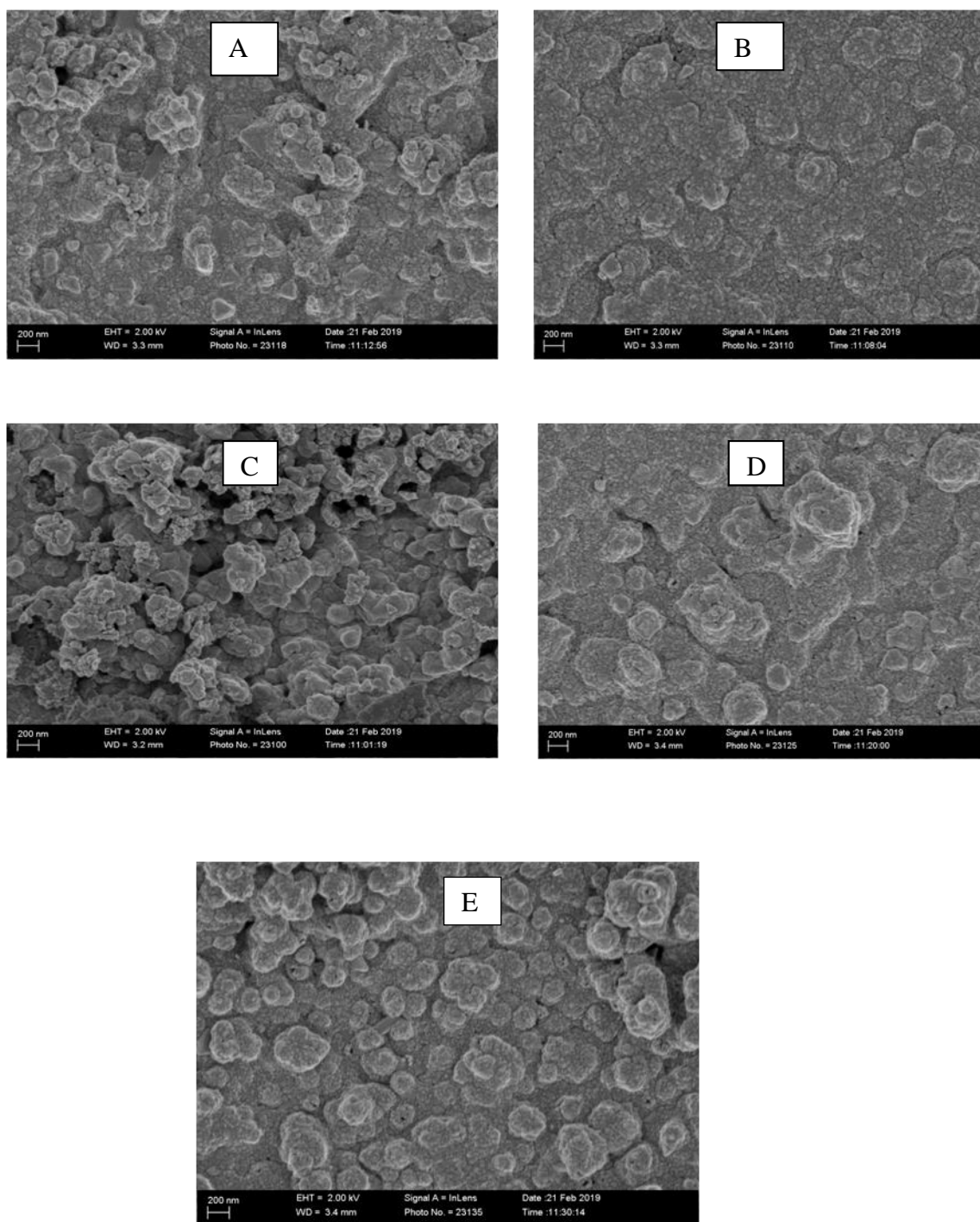


**Figure 4.12: SEM images for the samples anodized for (A) 1 min, (B) 2 min, (C) 3 min, (D) 10 min and (E) 30 min.**

The sample shown in Figure 4.12 (A) exhibited hilly like features which represents the formation of the metal oxide layer with porous structure, implying that Ti starts to be oxidized to  $Ti^{4+}$  ions at the surface layer of the Ti metal sample at this stage. Figure 4.12 (B) shows an almost compact and smooth surface morphology after anodization period of 2 min. It is interesting to note that by prolonging the anodizing time to 3 min, a layer of flower shaped features with irregular grains forms and covers the top layer of the  $TiO_2$  sample as seen in Figure 4.12 (C). Figure 4.12 (D) showed irregular grains with tiny cracks as samples are anodized for 10 min. In Figure 4.12 (E), the surface structure appears to be compact with formation of hill like structures in some sections of the sample. The entire cycle of grain and pore development is because of the electric field helped disintegration which is initiated under the applied potential, which in the end creates pores and grain-like structures. It is essential that field-helped oxidation and disintegration includes the development of an oxide layer and the disintegration of that oxide as well

#### **4.6 Photo-catalytic measurement**

The photocatalytic activities of the  $TiO_2$  tests are influenced by various factors, for example, average crystallite size, crystal structure, oxide film thickness and its chemical composition. Heterogeneous photocatalysis using  $TiO_2$  films is an advanced oxidant with a strong photocatalytic activity that absorbs large amounts of substances to be photodegraded on the surface of  $TiO_2$ . In this study, the fabricated samples were tested using a photo-catalytic reactor for a period of 40 min in a solution of water mixed with methylene blue as a representative of normal synthetic dyes. The rate of absorbance against time was recorded to determine the sample that best degrades the applied dye.

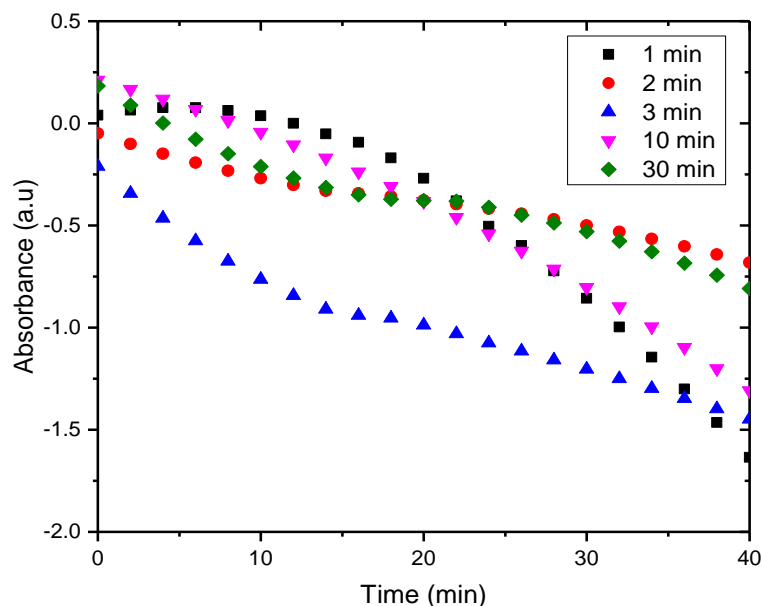


**Figure 4.13: Absorbance spectra for TiO<sub>2</sub> films anodized at different time intervals**

Figure 4.13 shows the absorbance spectra for TiO<sub>2</sub> films anodized at different time intervals. According to the figure, samples anodized for 1 min, 3 min, and 10 min displayed a decrease of methylene blue (MB) degradation in the presence of natural UV radiation from the sun as the time prolonged to 40 min. The sample anodized for 30 min showed an almost constant rate of degradation though with some degree of variation, sample anodized for 2 min had the best degradation rate of MB. It's reported that if the average crystallite size is small, the photocatalytic activity deteriorates because most of the interfaces become sink sites for the photo-excited charge carries of electrons and holes (Yoshiteru and Naoya, 2010). Furthermore, in small crystallines, electrons and holes cannot effectively separate as a result of the short migration distance hence resulting into a higher recombination rate of the charge carriers (Tanaka *et al*, 1991). Yoshiteru and



Naoya, (2010) further reports, that the rate of photodegradation of adsorbed substrates on the surface of the photocatalyst and its efficiency is lowered with increasing crystallite size. This is because of the inability of the photo-excited charge carriers to migrate to the surface of the photocatalyst because of an expansion in the recombination recurrence of the electron – hole pairs. Due to these two factors, an average crystallite size for photodegradation of MB dye should neither be too small nor big. In our study, the average crystallite size ( $D$ ) of 0.22 nm with the dislocation density ( $\delta$ ) and micro-strain ( $\epsilon$ ) of 20.7 and 0.166 respectively worked best in the photodegradation of MB dye compared to the others. Therefore, for sample anodized at 200 V, the optimum anodization time for better photodegradation of MB dye was found to be 2 min.

## CHAPTER FIVE

### CONCLUSION AND RECOMMENDATION

#### 5.1 Introduction

In this chapter, the summary of the research findings in accordance with the objectives of the study is outlined and the recommendation for further studies made known.

#### 5.2 Conclusion

TiO<sub>2</sub> films were successfully fabricated by anodization at 200V for different time intervals between 1 min to 30 min. Samples anodized between 1 min and 3 min exhibited different colors after which the change in terms of color became almost negligible. The change in colour is due to the interference of light reflected at the air-oxide interface and the light reflected at the metal substrate-oxide interface. This can be identified with the oxide layer development (thickness) on the example.

The surface, precious stone and optical properties of the examples demonstrated that there was an away from of the oxide layer on the Ti surface. Drawing out the anodization time engineered the formation of pores and eventual pore merging of the TiO<sub>2</sub> film thereby significantly influencing the surface morphology and crystallinity of the sample.

The XRD measurements for the crystal structure confirmed the coexistence of both rutile and anatase phases in TiO<sub>2</sub> samples anodized at 200 V, pigmented and annealed at a temperature of 450 °C for 4 hours.

The reflectance measurement showed that the Ti sample anodized at 2 min exhibited a higher oxide layer thickness of 125.14 nm compared to the other Ti samples.

The photocatalytic test showed that absorbance is affected by both the optical, crystal and surface properties of the anodic TiO<sub>2</sub> samples. The samples degraded the methylene blue solution at different rates.

Finally, the sample anodized for 2 min showed a stable photocatalytic process. This implies that absorbance increase with film thickness due to the change in film thickness, light catching or optical repression and consequently light retention of the examples.

### **5.3 Recommendation for further work**

Further work to be done in determining the effect of concentration of the anodization electrolyte, Anodic voltage and electrolyte temperature on the photocatalytic conduct of TiO<sub>2</sub> films.

## REFERENCE

- Akira, F. Xintong, Z. Donald, A. and Tryk, D. (2008), TiO<sub>2</sub> photocatalysis and related surface phenomena, *Surface Science Reports* **63**, 515-582.
- Akpan, U. and Hameed, B. (2009), Parameters affecting the photocatalytic degradation of dyes using TiO<sub>2</sub>-based photocatalysts: a review. *J Hazard Mater* **170(2-3)**, 520-529.
- Allam, N. Shankar, K. and Grimes, C. (2008), General method for the anodic formation of crystalline metal oxide nanotube arrays without the use of thermal annealing. *Adv Mater.* **20**, 3942-3946.
- Arconada, N. Duran, A. Suarez, S. Portela, R. Coronado, J. Sanchez, B. and Castro, Y. (2009), Synthesis and photocatalytic properties of dense and porous TiO<sub>2</sub> - anatase thin films prepared by sol-gel, *Appl. Catal. B Environ.* **86(1)**, 1-7.
- Bagheri, S. Chekin, F. and Hamid, S. (2014), Cobalt doped titanium dioxide nanoparticles: Synthesis, characterization and electrocatalytic study. *J. Chinese Chem. Soc.* **61**, 702 - 706.
- Beltran, A. Gracia, L. and Andres, J. (2006), *Journal of Phys. Chem. B*, **110**, 23417-23423.
- Batt, J. Milward, M. Chapple, I. Grant, M. Roberts, H. and Addison, O. (2018), *TiO<sub>2</sub> nanoparticles can selectively bind CXCL8 impacting on neutrophil chemotaxis*, *European Cells and Materials.* **35**, 13-24.

- Cernuto, G. Masciocchi, N. Cervellino, A. Colonna, G. and Guagliardi, A. (2011), Size and shape dependence of the photocatalytic activity of TiO<sub>2</sub> nanocrystals: a total scattering Debye function study. *J Am Chem Soc.***133(9)**, 3114–3119.
- Chan, S. Wu, T. Juan, J. and Teh, C. (2011), Recent developments of metal oxide semiconductors as photocatalysts in advanced oxidation processes (AOPs) for treatment of dye waste-water, *Journal of Chemical Technology & Biotechnology*, **86**, 1130–1158.
- Chatterjee, D. and Dasgupta, S. (2005), Visible light induced photocatalytic degradation of organic pollutants. *J Photochem Photobiol C.***6(2–3)**, 186–205.
- Chatzisyneon, E. Petrou, C. and Mantzavinos, D. (2013), photocatalytic treatment of textile dyehouse effluents with simulated and natural solar light. *Global NEST Journal*, **15(1)**, 21-28.
- Chinta, S. and VijayKumar, S. (2013), Technical facts and figures of reactive dyes used in textiles. *IJEMS.***4(3)**, 308-312.
- Chong, M. Jin, B. Chow, C. and Saint, C. (2010), recent developments in photocatalytic water treatment technology: A review, *Water Res.***44**, 2997–3027.
- Czoska, A. Livraghi, S. Chiesa, M. Giamello, E. Agnoli, S. Granozzi, G. Finazzi, E. and Di Valentin, C. (2008), Pacchioni G. *Journal of Physical Chemistry C.***112**, 8951–8956.

- Duong, H. Serpone, N. and Graetzel, M. (1984), Integrated Systems for Water Cleavage by Visible Light; Sensitization of Titanium Dioxide Particles by Surface Derivatization with Ruthenium Complexes *Helv. Chim. Acta*, **67**, 1012– 1018.
- Edwards, J. (1997), Coating and Surface Treatment Systems for Metals. *Finishing Publications Ltd. and ASM International*. 39–40.
- Foo, K. and Hameed, B. (2010), Decontamination of textile wastewater via TiO<sub>2</sub>/activated carbon composite materials. *Adv Colloid Interface Science*. **159(2)**, 130-143.
- Fujishima, A. Akira, F. Honda, G. and Kenichi, P. (1972), Electrochemical Photolysis of Water at a Semiconductor Electrode. *Nature*. **238(5358)**, 37– 38.
- Fujishima, A. Rao, T. and Tryk, D. (2000), Titanium dioxide photocatalysis. *J Photochem Photobiol C*. **1(1)**, 1 – 12.
- Gaya, U. and Abdullah, A. (2008), Heterogeneous photocatalytic degradation of organic contaminants over titanium dioxide: a review of fundamentals, progress and problems. *Journal of Photochemistry and Photobiology C: Photochemistry Reviews*, **9(1)**, 1-12.
- Gnanasekaran, L. Hemamalini, R. and Ravichandran, K. (2015), Synthesis and characterization of TiO<sub>2</sub> quantum dots for photocatalytic application. *J Saudi ChemSoc*. **19(5)**, 589–594.

- Gong, D. Grimes, C. Varghese, O. Hu, W. Sing, R. Chen, Z. and Dickey, E. (2001), Titanium oxide nanotube arrays prepared by anodic oxidation, *J.Mater.Res***16**, 3331.
- Gümüs, D. and Akbal, F. (2011), Photocatalytic degradation of textile dye and waste water, *Water Air & Soil Pollution*, **216**, 117 – 124.
- Habib, M. Shahadat, M. Bahadur, N. Ismail, I. and Mahmood, A. (2013), Synthesis and characterization of ZnO-TiO<sub>2</sub>nanacomposites and their application as photocatalysts. *Int Nano Lett*; **3(5)**, 1186.
- Hagen, J. (2006), Industrial catalysis: a practical approach/Jens Hagen, (2nd edn) Wiley, Weinheim.
- Han, G. Wang, L. Pei, C. Shi, R. Liu, B. Zhao, H. Yang, H. Liu, S. (2014), Size-dependent optical properties and enhanced visible light photocatalytic activity of wurtzite CdSe hexagonal nanoflakes with dominant 001 facets. *J Alloy Compd.***610**, 62–68.
- Hou, Y. Zhuang, D. Zhang, G. Zhao, M. and Wu, M. (2003), Influence of annealing temperature on the properties of titanium oxide thin film, *Applied Surface Science.***218**, 98-106.
- Hussein, M. and Assadi, N. (2016), The effects of copper doping on photocatalytic activity at (101) planes of anataseTiO<sub>2</sub>: A theoretical study. *Applied Surface Science.* **387**, 682–689.

- Joshi, M. Bansal, R. and Purwar, R. (2004), Color removal from textile effluents. *Indian J Fibre Text Res.***29**,239-59.
- Kang, Y. Young, T. Guang, J. and Wan, I. (1999), Photocatalytic Activity of Cu/TiO with oxidation State of Surface-loaded Copper, *Bull. Korean Chem. Soc.* **20(8)**, 957-960.
- Kalaivani, G. and Suja, S. (2016), TiO<sub>2</sub> (rutile) embedded inulin—A versatile bio-nano composite for photocatalytic degradation of methylene blue, *Carbohydr.Polym.***143**, 51–60.
- Kazeminezhad, I. and Sadollahkhani, A. (2016), Influence of pH on the photocatalytic activity of ZnO nanoparticles. *J Mater Sci Mater Electron.* **27(5)**, 4206–4215.
- Khan, M. Adil, S. and Al-Mayouf, A. (2015), Metal oxides as photocatalysts. *J Saudi Chem Soc.***19(5)**, 462–464.
- Kiriakidou, F. Kondarides, D. and Verykios, X. (1999), the effect of operational parameters and TiO<sub>2</sub>-doping on the photocatalytic degradation of azo-dyes. *Catal Today.***54**, 119–130.
- Konstantinou, K. and Triantafyllos, A. (2004), TiO<sub>2</sub>-assisted photocatalytic degradation of azo dyes in aqueous solution: Kinetic and mechanistic investigations. *Applied Catalysis B: Environmental.* **49**, 1.



- Kumar, N. Bogireddy, R. Kiran Kumar, H. and Mandal, B. (2016), Biofabricated silver nanoparticles as green catalyst in the degradation of different textile dyes, *J. Environ.Chem.Eng.***4**, 56–64.
- Liang, W. Jianhua, L. Mei, Y. Songmei, L. Hongxing, L. and Mengqi, Z. (2014), Effect of Anodization time on Morphology and Electrochemical Impedance of Andic Oxide Films on Titanium Alloy in Tartrate. *Int. J. Electrochem. Sci.* **9**, 5012 - 5024.
- Li, Y. Li, X. Li, J. and Yin, J. (2005), Photocatalytic degradation of methyl orange in a sparged tube reactor with TiO<sub>2</sub> coated activated carbon composite. *CatalCommun.***6(10)**, 651-55.
- Liu, G. Huang, W. and Yi, Y. (2013), Preparation and Optical Storage Properties of  $\lambda$ Ti<sub>3</sub>O<sub>5</sub> Powder. *Journal of Inorganic Materials (in Chinese)*. **28(4)**, 425–430.
- Li, X. and Zhang, M. (1996), Decolorization and biodegradability of dyeing wastewater treated by a TiO<sub>2</sub> sensitized photo-oxidation process, *Water Science & Technology*.**34**, 49–55.
- Maeda, M. and Yamada, T. (2007), Photocatalytic activity of metal-doped titanium oxide films prepared by sol-gel process, *Journal of Physics: Conference Series* **61**, 755–759.

- Malato, S. Fernández-Ibáñez, P. Maldonado, M. Blanco, J. Gernjak, W. (2009), Decontamination and disinfection of water by solar photocatalysis: *recent overview and trends. Catal Today.* **147(1)**, 1–59.
- Malekshahi, B. Nemati, K. Fatholahi, L. and Malekshahi, B. (2013), A Review on Synthesis of Nano-TiO<sub>2</sub> via Different Methods. *J.Nanostructures.***3**, 1-9.
- Muruganandham, M. Sobana, N. and Swaminathan, M. (2006), Solar assisted photocatalytic and photochemical degradation of Reactive Black 5, *Journal of Hazardous Materials.***137**, 1371–1376.
- Morikawa, T. Irokawa, Y. and Ohwaki, T. (2006), *Applied Catalysis A: General.***314**, 123–127.
- Nakane, J. Akenson, M. and Marziali, A. (2003), Nanopore sensors for nucleic acid analysis. *Topical Review.***15**, 1365-1393.
- Nakata, K. and Fujishima, A. (2012), TiO<sub>2</sub> photocatalysis: design and applications. *J PhotochemPhotobiol C.* **13(3)**, 169–189.
- Neppolian, B. Choi, H. Sakthivel, S. Arabindoo, B. and Murugesan, V. (2002), Solar light induced and TiO<sub>2</sub> assisted degradation of textile dye reactive blue 4. *Chemosphere* **46**, 1173–1181.
- Nolan, N. Seery, M. Hinder, S. Healy, L. and Pillai, S. (2010), *Journal of Physical Chemistry C.* **114**, 13026–13034.

- Novotny, C. Dias, N. Kapanen, A. Malachova, K. Vandrovцова, M. Itavaara, M. and Lima, N. (2006), Comparative use of bacterial, algal and protozoan tests to study toxicity of azo and anthraquinone dyes. *Chemosphere*. **63(9)**, 1436-42.
- Oganov, A. and Lyakhov, A. (2010), Towards the theory of hardness of materials. *Journal of Superhard Materials*. **32(3)**, 143–147.
- Ohno, T. Tokieda, K. Higashida, S. and Matsumura, M. (2003), *Appl. Catal.* **A244**, 383.
- Pearce, C. Lloyd, J. and Guthrie, J. (2003), The removal of colour from textile wastewater using whole bacterial cells: a review *Dye Pigm.* **58(3)**, 179-96.
- Punyasloka, P. Dangayach, G. and Awadhesh, K. (2018), A review on the sustainability of textile industries waste water with and without treatment methodologies, *Review, Environmental Health*, **33(2)**, 163 - 203
- Quan, X. Yang, S. Ruan, X. and Zhao, H. (2005), Preparation of titania nanotubes and their environmental applications as electrode, *Environ.Sci.Technol.* **39**, 3770-3775.
- Rajeshwar, K. Osugi, M. Chanmanee, W. Chenthamarakshan, C. Zaroni, M. Kajitvichyanukul, P. and Krishnan-Ayer, R. (2008), Heterogeneous photocatalytic treatment of organic dyes in air and aqueous media. *J Photochem Photobiol C*.**9(4)**:171–192.
- Rehman, S. Ullah, R. Butt, A. and Gohar, N. (2009), Strategies of making TiO<sub>2</sub> and ZnO visible light active. *J Hazard Mater.* **170(2–3)**, 560–569.

- Regonini, D. Bowen, C. Jaroenworarluck, K. and Stevens, R. (2013), A review of growth mechanism, structure and crystallinity of anodized TiO<sub>2</sub> nanotubes. *Mater. Sci. Eng. R* **74**, 377–406.
- Reza, K. Kurny, A. and Gulshan, F. (2015), Parameters affecting the photocatalytic degradation of dyes using TiO<sub>2</sub>: a review. *Appl. Water Sci.* doi:10.1007/s13201-015-0367-y.
- Saggiaro, E. Oliveira, A. Pavesi, T. Maia, C. Ferreira, L. and Moreira, J. (2011), Use of titanium dioxide photocatalysis on the remediation of model textile wastewaters containing azo dyes. *Molecules*. **16**, 10370-10386
- Sala, M. and Gutierrez-Bouzan, M. (2012), Electrochemical techniques in textile processes and wastewater treatment. *Int J Photoenergy*. 1-12.
- Saravanan, R. Gracia, F. and Stephen, A. (2017), Basic Principles, Mechanism, and Challenges of Photocatalysis, Nanocomposites for Visible Light-Induced Photocatalysis, 19 – 40.
- SharmilaDevi, R. Venckatech, R. and Sivaraj, R. (2014), Synthesis of titanium dioxide nanoparticles by sol-gel technique. *Int. J. Innov. Res. Sci. Eng. Technol.* **3(8)**, 15206 – 15211.
- Silva, C. and Faria, J. (2003), Photochemical and photocatalytic degradation of an azo dye in aqueous solution by UV irradiation, *Journal of Photochemistry and Photobiology A: Chemistry*. **155**, 133–143.

- Sohn, J. Lee, S. Cheon, P. and Kim, H. (2004), Acidic properties and catalytic activity of titanium sulfate supported on TiO<sub>2</sub>. *Bull. Korean Chem. Soc.* **25**, 657-664.
- Skoog, D. Holler, F. and Crouch, S. (2011), instrumental analysis (6<sup>th</sup> ed.). *Brooks Cole, Belmont*, 1039.
- Sul, Y. Johansson, C. Jeong, Y. and Albrektsson, T. (2001), Medical Engineering & Physics **23**, 329.
- Tanaka, K. Capule, M. and Hisanaga, T. (1991), *Chem. Phys. Lett.* **187**, 73–76.
- Trivedi, M. Ameta, C. Solanki, S. Ameta, R. and Benjamin, S. (2015), Use of Cu-C-TiO<sub>2</sub> in dye sensitized Solar cell. *International Journey of Scientific and Technology Research.* **4(7)**, 135-140.
- Wang, K. Chen, H. Huang, L. Su, Y. and Chang, S. (2008), Degradation of Reactive Black 5 using combined electrochemical degradation-solar-light/immobilized TiO<sub>2</sub> film process and toxicity evaluation, *Chemosphere*, **72**, 299–305.
- Wesenberg, D. Kyriakides, I. and Agathos, S. (2003), White-rot fungi and their enzymes for the treatment of industrial dye effluents. *Biotechnol Adv.* **22(1-2)**:161-87.
- Ye, Q. Liu, P. Tang, Z. and Zhai, L. (2007), “Hydrophilic properties of nano-TiO thin films deposited by RF magnetron sputtering,” *Vacuum.* **81**, 627-631.
-

Yoshiteru, M. and Naoya, M. (2010), Photocatalytic Activities and Crystal Structures of Titanium Dioxide by Anodization: Their Dependence upon Current Density *Materials Transactions*.**51(8)**, 1443-1448.

Zhang, X. Zhou, M. and Lei, L. (2005), Preparation of photocatalytic TiO<sub>2</sub> coatings of nano-sized particles on activated carbon by APMOCVD. *Carbon*.**43(8)**, 1700-1708.

## APPENDIX I : SIMILARITY REPORT

Turnitin

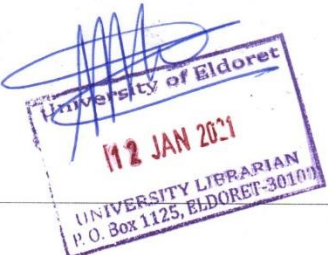
[https://www.turnitin.com/newreport\\_classic.asp?lang=en\\_us&o...](https://www.turnitin.com/newreport_classic.asp?lang=en_us&o...)

Document Viewer

### Turnitin Originality Report

Processed on: 12-Jan-2021 15:34 EAT  
 ID: 1486274021  
 Word Count: 18676  
 Submitted: 1

SC/PGP/007/15 By Peter Owino



Similarity Index	Similarity by Source
18%	Internet Sources: 11% Publications: 11% Student Papers: 6%

include quoted   
  include bibliography   
  excluding matches < 5 words   
 mode:

3% match (publications) Sumathi Suresh. "Treatment of Textile Dye Containing Effluents", Current Environmental Engineering, 2015	✕
1% match (student papers from 13-Feb-2018) Submitted to University of Kabianga on 2018-02-13	✕
1% match (Internet from 03-May-2020) <a href="https://pt.scribd.com/document/278001945/Optical-Properties-of-Dielectric-Films">https://pt.scribd.com/document/278001945/Optical-Properties-of-Dielectric-Films</a>	✕
<1% match (Internet from 28-Oct-2020) <a href="https://link.springer.com/chapter/10.1007/978-3-319-62446-4_2">https://link.springer.com/chapter/10.1007/978-3-319-62446-4_2</a>	✕
<1% match (publications) Subhasish Chatterjee, Miriam Ginzberg, Bonnie Gersten. " Effect of anodization conditions on the synthesis of TiO nanopores ", MRS Proceedings, 2011	✕
<1% match (publications) "Surgical Tools and Medical Devices", Springer Science and Business Media LLC, 2016	✕
<1% match () <a href="http://eprints.usm.my">http://eprints.usm.my</a>	✕
<1% match (student papers from 22-Aug-2011) Submitted to University of Glasgow on 2011-08-22	✕
<1% match (Internet from 11-Aug-2019) <a href="https://mafiadoc.com/evaluation-of-the-energy-performance-and-design-citeseerx_597892a51723dde38bd39ab7.html">https://mafiadoc.com/evaluation-of-the-energy-performance-and-design-citeseerx_597892a51723dde38bd39ab7.html</a>	✕